Generalized hydrodynamics and the acoustic modes of water: Theory and simulation results

Davide Bertolini
Istituto di Fisica Atomica e Molecolare del Consiglio Nazionale delle Ricerche, Via del Giardino 7, I-56100 Pisa, Italy

Alessandro Tani*
Dipartimento di Chimica dell'Università di Pisa, Via Risorgimento 35, I-56126 Pisa, Italy
(Received 31 January 1994; revised manuscript received 16 September 1994)

We discuss an application of extended hydrodynamics to a model of water, in a range of wave numbers k, where the effect of single-molecule modes must be taken into account together with the collective phenomena underlying sound propagation and dispersion. The calculation of the density-density, energy-density, energy-energy, and longitudinal and transverse current correlation functions from a molecular dynamics simulation of the transferable intermolecular potential with four points (TIP4P) model of water, allows us to obtain the k dependence of the generalized hydrodynamic coefficients. In particular, we have found that the ratio of generalized heat capacities $\gamma(k)=c_p(k)/c_v(k)\cong 1$ up to $k\cong 1$ Å^{-1} and that the correlation between temperature and density fluctuations is negligible at all times, while there is an important frequency dependence of the transport coefficients. This leads to a remarkable simplification of the expression of the Laplace transform of the correlation functions, although models for the transport coefficients are still necessary at the present state of the theory. The frequency dependence of the transport coefficients is necessary to describe correctly the behavior of the density-density and temperature-temperature autocorrelation functions (ACF's). A model for the frequency dependence of the generalized viscosity $\tilde{\phi}(k,z)$ and thermal diffusivity $\tilde{D}_T(k,z)$ is proposed here. In addition to the correct short-time behavior of the correlation functions of the memory kernel, this model is able to account satisfactorily for the effects of the acoustic mode and the single-molecule modes, in particular, that related to the oscillation in the nearest neighbor cage (45 THz). A simple polynomial extrapolation to $k=0$ of the parameters of the model gives values consistent with the large sound dispersion observed in water. In the supercooled region, the shape of the predicted dispersion curve shows that there are two k ranges, 0.01–0.03 and 0.2–0.5 Å^{-1}, which account for most of the dispersion. When the temperature increases the contribution to the lower k range is less apparent and shifted to higher k, but the behavior of the 0.2–0.5 Å^{-1} range does not change. The model also predicts an acoustic mode frequency $\omega_{\max}(k)/k$, 2–3 times larger, and a bandwidth $\Delta\omega_{1/2}(k)/k^2$, almost an order of magnitude smaller than those in the hydrodynamic regime. Moreover, $\omega_{\max}(k)$ and $\Delta\omega_{1/2}(k)$ are in quantitative agreement with the neutron scattering data at $T=298$ K. The location and height of the first step of the dispersion curve are related to the long-time tail of generalized viscosity, while its size is determined by the anomalous value of the second moment of the longitudinal current $\omega_\infty(k)$ as compared to that of the density-density ACF $\omega_0(k)$. The analysis of the transverse current ACF with the same model and the value of the transport coefficients obtained confirm that the TIP4P model potential leads to a shear and bulk viscosity in satisfactory agreement with the experimental data at 298 K. In the supercooled region, conversely, the dynamics obtained with the TIP4P potential is 2–3 times faster than that of real water at the same temperature, as already noted for the self-diffusion coefficient and dielectric relaxation times.

PACS number(s): 61.20.Gy, 61.25.−f, 62.60.+v

I. INTRODUCTION

Over the past decade there has been a debate in the literature on the physical mechanism underlying a velocity of sound in water roughly twice as large, in the range $0.25<k<1$ Å^{-1}, as that in the hydrodynamic, $k\to 0$, regime. This was observed both by molecular dynamics (MD) computer simulation [1,2] and by inelastic neutron scattering experiments [3]. These data have been explained either as evidence of a second acoustic mode that propagates through the hydrogen bond network with a speed close to that in ordinary ice [4,5] or as a consequence of anomalous positive dispersion of the normal acoustic mode [6,7].

Recent simulation results [8–10] support the latter hypothesis. Actually, it has been shown in [8] that one of the two peaks in the spectrum of the density-density autocorrelation function (ACF), for water modeled by the Stillinger and Rahman ST2 potential [1,5], is due to a single-molecule mode rather than to a second high-frequency sound mode. On the other hand, Balucani *et al.* [9,10] have proven that the large sound dispersion is to be traced to the anomalous, very large value of the second moment of the longitudinal current compared to that of density-density ACF. This has been related to the structure of water and in particular to the distance of the

*Author to whom correspondence should be addressed.

main peak of the oxygen-oxygen radial distribution function $g_{00}(r)$, determined by the directionality of the hydrogen bond and the tetrahedral arrangement of molecules in the network.

In order to interpret their simulation results obtained with the Matsuoka-Clementi-Yoshimine model intermolecular potential, Wojcik and Clementi [6] fitted the spectrum of density-density ACF with a model proposed by Levesque *et al.* [11,12] to analyze their simulation data of liquid argon. This attempt has shown that the observed behavior is consistent with a large sound dispersion. However, as the dependence on k of some hydrodynamic coefficients was unknown, Wojcik and Clementi were forced to some assumptions and concluded that this model reproduces fairly well the central peak of the dynamic structure factor, but shows some drawbacks concerning the side peaks, i.e., those relevant to sound propagation.

If the hypothesis of a large dispersion of ordinary sound is correct, generalized hydrodynamics [13–15] should provide useful insight and this is why we attempt to apply this approach to the overall dynamic behavior of water, in the spirit of two fairly recent works [16,17].

Then, in our analysis we not only calculate the density-density correlation functions (CF's) but also the energy-density and energy-energy CF's in addition to longitudinal and transverse current CF's at 245 K, for several values of k. To investigate the temperature effect, the density-density, longitudinal, and transverse current CF's have been calculated at 298 K.

The equal time values of this set of correlation functions allow us to obtain the generalized enthalpy $h(k)$, constant volume and pressure heat capacity $c_v(k)$ and $c_p(k)$, their ratio $\gamma(k)$, and the thermal expansivity $\alpha(k)$. We emphasize that the calculation of energy-energy and energy-density CF's, in addition to the density-density CF, and the knowledge of the k dependence of the thermodynamic functions, in particular, $\gamma(k)$, besides their interest *per se,* also eliminates the risk of an incorrect interpretation of the physical meaning of the parameters that enter a fitting function for the time dependence of the density-density CF (see Sec. IV B).

de Schepper *et al.* [17] have shown that, for the Lennard-Jones (LJ) liquid, the evaluation of the three independent correlation functions (density-density, energy-density, and energy-energy) allows a complete description of the longitudinal dynamics. In other words, the time dependence of all 25 CF's based on the five fundamental quantities, i.e., the longitudinal velocity u, the longitudinal stress tensor σ, and the longitudinal heat flux q, in addition to the density n and energy e, can be described as a linear combination of five exponentials. The time domain approach coincides with the more general, formally exact, frequency domain approach when the coefficients of the linear combination do not depend on time [17]. This cannot be assumed to hold in the case of water and even for simple LJ liquids and liquid metals, at least in some thermodynamic states, whenever the time dependence of the generalized viscosity $\phi(k,t)$ requires two separated time scales to be correctly described [11,12,18]. Therefore, we work in the frequency domain to obtain the generalized thermodynamic properties and transport parameters necessary to describe the dynamics of the system, using Laplace transforms of correlation functions of orthonormal combination of the five fundamental variables relevant to the longitudinal dynamics [17].

In order to reach a correct description of the normalized density-density and temperature-temperature ACF's, it is necessary to take into account the frequency dependence of the transport coefficients. Many papers, mainly concerning the viscoelastic theory [19–22], have stressed the importance of this approach to generalize linear hydrodynamics. Moreover, the spectrum of the velocity ACF has been related [23] to the frequency-dependent friction coefficient, which is proportional to the viscosity in the Stokes-Einstein formula. This relation is particularly important when the velocity ACF has a long-time tail, e.g., in argon close to the triple point or in water below room temperature. In these thermodynamic states, it is apparent that, in argon [12], rubidium [21], and water [10], the time dependence of the generalized viscosity shows two well separated time scales. As a consequence, the simulation results cannot be described correctly by a simple exponential dependence of the generalized viscosity.

In the case of water, the spectrum of the velocity ACF displays two main peaks, one (45 THz) relevant to the oscillation in the cage of the nearest neighbors, whose amplitude increases when temperature is lowered, and a lower frequency band (9–10 THz) generally considered a O—O—O bending mode [2,5,8,24].

Any model to be used in the description of the generalized transport parameters of water should take these self-modes into account, especially at those k values where the acoustic mode frequencies become of the same order of magnitude as the self-modes, which depend weakly on k. Hence the theoretical approach introduced, which supplements traditional hydrodynamics with information on generalized viscosity, from the longitudinal stress tensor fluctuations, and thermal diffusivity, from longitudinal heat flux fluctuations, should provide useful insight both on single-molecule dynamics and on the influence of long-time tails on the collective dynamics.

This paper is organized as follows. Computational details on the simulations we carried out are collected in Sec. II. Section III is devoted to a brief outline of the theory. Section III A contains a discussion of the problems inherent to the extension of generalized hydrodynamics to molecular liquids and of the approximations we adopted, while Sec. III B recalls the main results required to analyze the simulation results. The latter are presented in Sec. IV, where the behavior of the generalized thermodynamic quantities is discussed and the importance of the frequency dependence of the transport parameters is stressed. In Sec. V we present a model for the transport parameters that is applied first to longitudinal dynamics, analyzing the anomalous sound dispersion (Sec. VI), the longitudinal stress tensor, heat flux fluctuations (Sec. VII), and the relation between collective and individual dynamics and the long-time tails behavior (Sec. VIII). In Sec. IX the model is also applied to transverse currents. Finally, the various transport coefficients

(viscosity, shear modulus, and thermal conductivity) are extrapolated to $k=0$, to compare the calculated values to the experimental data (Sec. X). Section XI summarizes our results.

II. COMPUTATIONAL DETAILS AND OBSERVED DYNAMIC VARIABLES

The results we present in this paper have been obtained from an analysis of the trajectories produced by a molecular dynamics simulation, in the microcanonical ensemble, of the transferable intermolecular potential with four points (TIP4P) model of water [25] on a sample of 343 molecules in a cubic box with periodic boundary conditions in the usual minimum image convention. The short-range Lennard-Jones part of the TIP4P potential has been spherically truncated at half the box side, i.e., $r_c=10.9$ Å. Long-range corrections have been applied to both the internal energy and the virial sum, replacing the radial distribution function with 1 beyond the cutoff distance r_c.

The equations of motion have been integrated with the generalized method of constraints [26], with time steps of 2.0 and 2.5 fs at 298 and 245 K, respectively, fairly usual values for rigid models of small molecules. The use of the method of constraints and of Ewald sums allowed very good energy conservation, with no upward or downward drift and fluctuations no larger than $10^{-2}\%$. Also, no velocity rescaling was required to maintain average temperature at the desired value.

The length of the runs reported in Table I relates to the number of steps performed starting from very well equilibrated configurations from previous work [24,27]. The thermodynamic data obtained in the present work reproduce quantitatively those computed in [24]. All k-dependent time correlation functions have been averaged over all k vectors of the same magnitude. Other details on the runs and the computed CF's are given in Table I.

To reduce truncation effects in the Laplace transforms, we have fitted the time correlation functions with a linear combination of exponentials with complex coefficients, in the spirit of what done for argon [17]. These functions allow us to obtain very accurate fits, although the physical meaning of the optimized parameters is difficult to extract because the frequency dependence of the transport parameters is important. The difference between the time correlation function and the fitting function is then numerically transformed and the result added to the analytical transform of the fitting function.

TABLE I. Details of the simulation runs. The subscripts of the correlation functions relate to density (1), longitudinal velocity (2), and energy (3) (see text). $C_\perp$ is the transverse current ACF.

Run	T (K)	$N/10^3$	Δt (ps)	Correlation functions
1	245	52	0.0025	$F_{11},F_{22},C_\perp$
2	245	66.5	0.0025	$F_{11},F_{22},F_{13},F_{33}$
3	298	40	0.002	$F_{11},F_{22},C_\perp$

The Laplace transform of the normalized longitudinal current ACF's, $G_{22}(k,t)$, which have been computed independently and suffer smaller truncation effects, have been used as a check of the numerical procedure. The comparison with the transform of the normalized density-density ACF's, $G_{11}(k,t)$, is done through the well known relation

$$G_{22}(k,\omega)=\frac{\omega^2 G_{11}(k,\omega)}{f_{un}(k)^2}\ , \tag{2.1}$$

where

$$G_{jl}(k,\omega)\equiv \mathrm{Re}\{\tilde{G}_{jl}(k,z)\} = \mathrm{Re}\left\{\int_0^\infty dt\, e^{-zt} G_{jl}(k,t)\right\}\ . \tag{2.2}$$

The relation (2.1) is very well satisfied at all frequencies and for the k range explored. $G_{22}(k,\omega)$ is more accurate at the highest frequencies ($\omega>30$ THz) and can be used to correct $\omega^2 G_{11}(k,\omega)$. In the low-frequency region, on the other hand, $G_{11}(k,\omega)$ is more accurate, so the most effective fitting procedure relies on a linear combination of the two functions, namely, $(1+\delta\omega^2)G_{11}(k,\omega)$ with $0\le\delta\le 1$ ps^2. It should be noted that when $\delta=1/f_{un}(k)^2$, this linear combination becomes $G_{11}(k,\omega)+G_{22}(k,\omega)$ [Eq. (2.1)].

III. GENERALIZED HYDRODYNAMICS EQUATIONS AND TRANSPORT COEFFICIENTS

A. Theory and approximations adopted

We give here just a brief outline of the theory, which is described in detail in [17], keeping the same notation for the sake of convenience. As already mentioned, the 25 time derivative of CF's, $F_{jl}(k,t)$, can be obtained from the five fundamental quantities density, longitudinal velocity, energy, longitudinal stress tensor, and longitudinal heat flux. We number the above quantities from 1 (density) to 5 and define the time CF's as

$$F_{jl}(k,t)=\langle a_j(\mathbf{k})^* a_l(\mathbf{k},t)\rangle\ . \tag{3.1}$$

The five microscopic quantities $a_j(\mathbf{k})$ are defined as

$$a_j(\mathbf{k})=\frac{1}{\sqrt{N}}\sum_{l=1}^{N} A_j^{(l)}(\mathbf{k}) e^{-i\mathbf{k}\cdot\mathbf{r}^{(l)}}\ , \tag{3.2}$$

where the index (l) relates to the molecules and

$$A_1^{(l)}(\mathbf{k})=1 \tag{3.3}$$

for density ($j=1$),

$$A_2^{(l)}(\mathbf{k})=\mathbf{v}^{(l)}\cdot\mathbf{k}/k \tag{3.4}$$

for longitudinal velocity ($j=2$),

$$A_3^{(l)}(\mathbf{k})=\tfrac{1}{2}m v^{(l)2}+\tfrac{1}{2}\sum_{n=1\neq l}^{N}\phi(\mathbf{r}^{(ln)},r_c) \tag{3.5}$$

for energy density ($j=3$),

$$A_4^{(l)}(\mathbf{k})=(\mathbf{v}^{(l)}\cdot\mathbf{k}/k)^2 + \frac{i}{2mk^2}\sum_{n=1\neq l}^{N}\mathbf{k}\cdot\frac{\partial\phi}{\partial\mathbf{r}^{(ln)}}(e^{-i\mathbf{k}\cdot\mathbf{r}^{(ln)}}-1) \tag{3.6}$$

for longitudinal momentum flux ($j=4$), and

$$A_5^{(l)}(\mathbf{k})=\left\{\frac{1}{2}mv^{(l)2}+\frac{1}{2}\sum_{n=1\neq l}^{N}\phi\right\}(\mathbf{v}^{(l)}\cdot\mathbf{k}/k) + \frac{i}{2k}\sum_{n=1\neq l}^{N}\mathbf{v}^{(l)}\cdot\frac{\partial\phi}{\partial\mathbf{r}^{(ln)}}(e^{-i\mathbf{k}\cdot\mathbf{r}^{(ln)}}-1) \tag{3.7}$$

for longitudinal heat flux ($j=5$).

Equations (3.3)–(3.7) are written for an atomic fluid. Hence an extension of these definitions to a molecular liquid such as water would require replacing the center of mass position and velocity with that of all three atoms, so that for $j=1$ there should be three phase factors, for $j=2$ three velocities, and for ($j=3$) additional summations extended to the three velocities and the four interaction centers, as the TIP4P potential [25,28,29] depends on the charges position for the Coulomb part and on the oxygen position for the short-range Lennard-Jones part. Relatively few attempts to extend generalized hydrodynamics to molecular liquids have been made [30–32].

Furthermore, the main interest of this work relates to relatively slow modes (<70 THz), due to the center of mass dynamics, especially in the low-k region [33]. Hence we have chosen a mixed description, whereby all phase factors and velocities correspond to the center of mass, while the potential energy $E_{\rm pot}$ contains all atom-atom and charge-charge contributions required by the TIP4P model.

For a molecular liquid such as water, described as a set of rigid molecules, the total energy can be written as

$$A_3^{(l)}(\mathbf{k})=\tfrac{1}{2}mv^{(l)2}+\tfrac{1}{2}\sum_i I_i^{(l)}\omega_i^{(l)2}+E_{\rm pot}\ , \tag{3.8}$$

where $I_i^{(l)}$ and $\omega_i^{(l)}$ are the moment of inertia and the angular velocity relative to the ith principal axis of inertia. As a consequence, the energy-energy correlation function contains a number of terms of rather different weight. We could check that the $\langle E_{\rm pot}E_{\rm pot}(t)\rangle$ contribution is, by far, the largest at both temperatures. On the contrary, rototranslational coupling has been shown [2,33,34] to be negligible compared to translational-translational and rotational-rotational terms. The latter can be further decomposed into a very rapid librational motion plus a much slower reorientational dipolar motion.

The librational motion can easily be eliminated from $F_{33}(k,t)$ (see Sec. IV and Table III) without affecting this CF in the part relevant to our analysis. As to the reorientational terms, again the potential part, which is included in $E_{\rm pot}$, dominates the kinetic one. Hence it seems sensible to neglect the second contribution on the right-hand side of Eq. (3.8) and maintain an atomiclike description of the kinetic terms, at least as far as the first three variables above are concerned [Eqs. (3.3)–(3.5)].

To verify this hypothesis, generalized thermodynamic variables such as $h(k)$, $c_v(k)$, and $\alpha(k)$ have been computed from CF's which include or neglect the rotational kinetic term. The values we obtain in the $k\to0$ limit are in a much better agreement with the corresponding ordinary thermodynamic variable, i.e., h, c_v, and α [24,28], when they are obtained without rotational contributions to kinetic energy (see, e.g., Fig. 8). These approximations we adopted rely on the very different time scales [33,34] of the acoustic modes (which we are mainly interested in here) with respect to the other motions and on the much larger size of the potential contribution to the energy compared to the kinetic one.

Finally, work in progress [35] on $F_{44}(k,t)$ shows that the model for the transport coefficients, based on the results of our approximate description, leads to a prediction of the CF for both diagonal and off-diagonal components of the stress tensor in quite satisfactory agreement with the results we obtain with the correct calculation in the $k\to0$ limit.

B. Initial values and calculation of the generalized hydrodynamic coefficients

The initial values and the short-time behavior of the CF's $F_{jl}(k,t)$ are the necessary information to calculate, according to the theory of critical phenomena [36–38], the generalized thermodynamic coefficients; see Eqs. (2.15)–(2.18) in Sec. II C in Ref. [17]. Defining the initial value

$$V_{jl}(k)\equiv F_{jl}(k,0)\ , \tag{3.9}$$

these relations are

$$\alpha(k)=\frac{h(k)V_{11}(k)-V_{13}(k)}{k_BT^2}\ , \tag{3.10}$$

$$c_v(k)=\frac{V_{33}(k)-\dfrac{V_{13}(k)^2}{V_{11}(k)}}{k_BT^2}\ , \tag{3.11}$$

$$c_p(k)=\frac{h(k)^2V_{11}(k)-2h(k)V_{13}(k)+V_{33}(k)}{k_BT^2}\ , \tag{3.12}$$

$$\gamma(k)=1+\frac{[h(k)V_{11}(k)-V_{13}(k)]^2}{V_{11}(k)\left[V_{33}(k)-\dfrac{V_{13}(k)^2}{V_{11}(k)}\right]}\ , \tag{3.13}$$

where

$$h(k)=-\frac{m}{k_BTk^2}\lim_{t\to0}\frac{\partial^2F_{13}(k,t)}{\partial^2t} \tag{3.14}$$

is the generalized enthalpy per molecule.

C. Orthonormal variables' ACF's and their properties

As shown in [17], it seems more convenient to introduce a new set of orthonormal variables $b_j(\mathbf{k})$ and linear combination of $a_j(\mathbf{k})$, whose time correlation functions can be defined as in Eq. (3.1)

$$G_{jl}(k,t)=\langle b_j(\mathbf{k})^*b_l(\mathbf{k},t)\rangle \tag{3.15}$$

and became linear combinations of the $F_{jl}(k,t)$. We give in the following the expression for $G_{11}(k,t)$, $G_{22}(k,t)$, $G_{13}(k,t)$, and $G_{33}(k,t)$:

$$G_{11}(k,t)=\frac{F_{11}(k,t)}{V_{11}(k)} , \tag{3.16}$$

$$G_{22}(k,t)=\frac{F_{22}(k,t)}{V_{22}(k)} , \tag{3.17}$$

$$G_{13}(k,t)=\frac{\left[F_{13}(k,t)-V_{13}(k)\frac{F_{11}(k,t)}{V_{11}(k)}\right]}{\left\{V_{11}(k)\left[V_{33}(k)-\frac{V_{13}(k)^2}{V_{11}(k)}\right]\right\}^{1/2}} , \tag{3.18}$$

$$G_{33}(k,t)=\frac{\left\{\left[\frac{V_{13}(k)}{V_{11}(k)}\right]^2 F_{11}(k,t)-2\frac{V_{13}(k)}{V_{11}(k)}F_{13}(k,t)+F_{33}(k,t)\right\}}{\left[V_{33}(k)-\frac{V_{13}(k)^2}{V_{11}(k)}\right]} . \tag{3.19}$$

Defining the Laplace transform of Eq. (3.15) as in Eq. (2.2), the following set of formally exact equations can be obtained [17]:

$$z\tilde{G}_{jl}(k,z)=-\sum_{n=1}^{5} H_{jn}(k,z)\tilde{G}_{nl}(k,z)+\delta_{jl} \quad (j,l=1,\ldots,5) . \tag{3.20}$$

$\underline{H}(k,z)$ is a symmetric matrix which is a function of four independent combinations of the coefficients $V_{jl}(k)$, the $f_{un}(k)$, $f_{u\sigma}(k)$, $f_{uT}(k)$, and $f_{Tq}(k)$ [see Eq. (2.28) of Ref. [17]], and of three generalized transport coefficients $z_\sigma(k,z)$, $z_q(k,z)$, and $z_{q\sigma}(k,z)$, formally expressed in Appendix A of [17]:

$$\underline{H}(k,z)=\begin{vmatrix} 0 & if_{un}(k) & 0 & 0 & 0 \\ if_{un}(k) & 0 & if_{uT}(k) & if_{u\sigma}(k) & 0 \\ 0 & if_{uT}(k) & 0 & 0 & if_{Tq}(k) \\ 0 & if_{u\sigma}(k) & 0 & z_\sigma(k,z) & iz_{q\sigma}(k,z) \\ 0 & 0 & if_{Tq}(k) & iz_{q\sigma}(k,z) & z_q(k,z) \end{vmatrix} . \tag{3.21}$$

It should be noted that no approximation is required to obtain Eq. (3.20), while to transform it back in time

$$\frac{\partial G_{jl}(k,t)}{\partial t}=-\sum_{n=1}^{5} H_{jn}(k)G_{nl}(k,t) \quad (j,l=1,\ldots,5) \tag{3.22}$$

it is necessary that z_σ, z_q, and $z_{q\sigma}$ do not depend on frequency.

From the relation (3.20), the 25 spectra of the time correlation functions $\tilde{G}_{jl}(k,z)$ can be computed as a function of the elements of $\underline{H}(k,z)$. We report here the results that relate $\tilde{G}_{11}(k,z)$, $\tilde{G}_{13}(k,z)$, $\tilde{G}_{33}(k,z)$, $\tilde{G}_{44}(k,z)$, and $\tilde{G}_{55}(k,z)$ to the elements of the matrix $\underline{H}(k,z)$:

$$\tilde{G}_{11}(k,z)=\cfrac{1}{z+\cfrac{f_{un}(k)^2}{z+z_\phi(k,z)+\cfrac{[f_{uT}(k)+\Delta(k,z)]^2}{z+z_T(k,z)}}} , \tag{3.23}$$

$$\tilde{G}_{13}(k,z)=\frac{-f_{un}(k)[f_{uT}(k)+\Delta(k,z)]}{D(k,z)} , \tag{3.24}$$

$$\tilde{G}_{33}(k,z)=\frac{[z^2+z_\phi(k,z)z+f_{un}(k)^2]}{D(k,z)} , \tag{3.25}$$

$$\tilde{G}_{44}(k,z)=\frac{\{[z+z_T(k,z)][z^2+f_{un}(k)^2]+zf_{uT}(k)^2\}}{\left\{[z+z_\sigma(k,z)]+\frac{z_{q\sigma}(k,z)^2}{[z+z_q(k,z)]}\right\}D(k,z)} , \tag{3.26}$$

$$\tilde{G}_{55}(k,z)=\frac{z[z^2+z_\phi(k,z)z+f_{un}(k)^2+f_{uT}(k)^2]}{\left\{[z+z_q(k,z)]+\frac{z_{q\sigma}(k,z)^2}{[z+z_\sigma(k,z)]}\right\}D(k,z)} , \tag{3.27}$$

where

$$D(k,z)=\{[z+z_T(k,z)][z^2+z_\phi(k,z)z+f_{un}(k)^2]+z[f_{uT}(k)+\Delta(k,z)]^2\} \tag{3.28}$$

and $z_\phi(k,z)$, $z_T(k,z)$, and $\Delta(k,z)$ are defined in Sec. IV B of Ref. [17]. We notice that they are proportional to $f_{u\sigma}(k)^2$, $f_{Tq}(k)^2$ and the product $f_{u\sigma}(k)f_{Tq}(k)z_{q\sigma}(k,z)$, respectively.

With the short-time values of the time correlation

functions $F_{11}(k,t)$, $F_{22}(k,t)$, $F_{13}(k,t)$, and $F_{33}(k,t)$ it is possible to calculate every element of the hydrodynamic matrix, except the three transport coefficients $z_\sigma(k,z)$, $z_q(k,z)$, and $z_{q\sigma}(k,z)$. The latter, as shown in Appendix A of [17], can be considered the Laplace transforms of a set of time correlation functions $J_\sigma(k,t)$, $J_q(k,t)$, and $J_{q\sigma}(k,t)$.

The z dependence of these generalized transport coefficients must be taken into account unless the relaxation time of $J_q(k,t)$, $J_\sigma(k,t)$, and $J_{q\sigma}(k,t)$ is much smaller than that of $G_{jl}(k,t)$. Only when this condition is satisfied can Eq. (3.20) be inverted to obtain Eq. (3.22). Finally, we note that the CF's $G_{11}(k,t)$, $G_{13}(k,t)$, and $G_{33}(k,t)$ can be derived from simulation data for $F_{11}(k,t)$, $F_{13}(k,t)$, and $F_{33}(k,t)$, using Eqs. (3.16)–(3.19).

IV. SIMULATION RESULTS

The time correlation functions $F_{11}(k,t)$ and $F_{22}(k,t)$, computed at various values of k for $T=245$ and 298 K, are shown in Figs. 1 and 2. To give an idea of the statistical uncertainty of the calculation, the functions obtained in the first and the second simulation of Table I are compared in Fig. 3 at $k=k_{\min}$.

$F_{13}(k,t)$ and $F_{33}(k,t)$ at $T=245$ K are plotted in Fig. 4. An additional simulation run where the energy included the rotational part was also carried out and the results are displayed in Figs. 4(e) and 4(f). Figure 5 shows the results for the transverse current CF's at both temperatures.

As expected, the short-time oscillation, typical of libra-

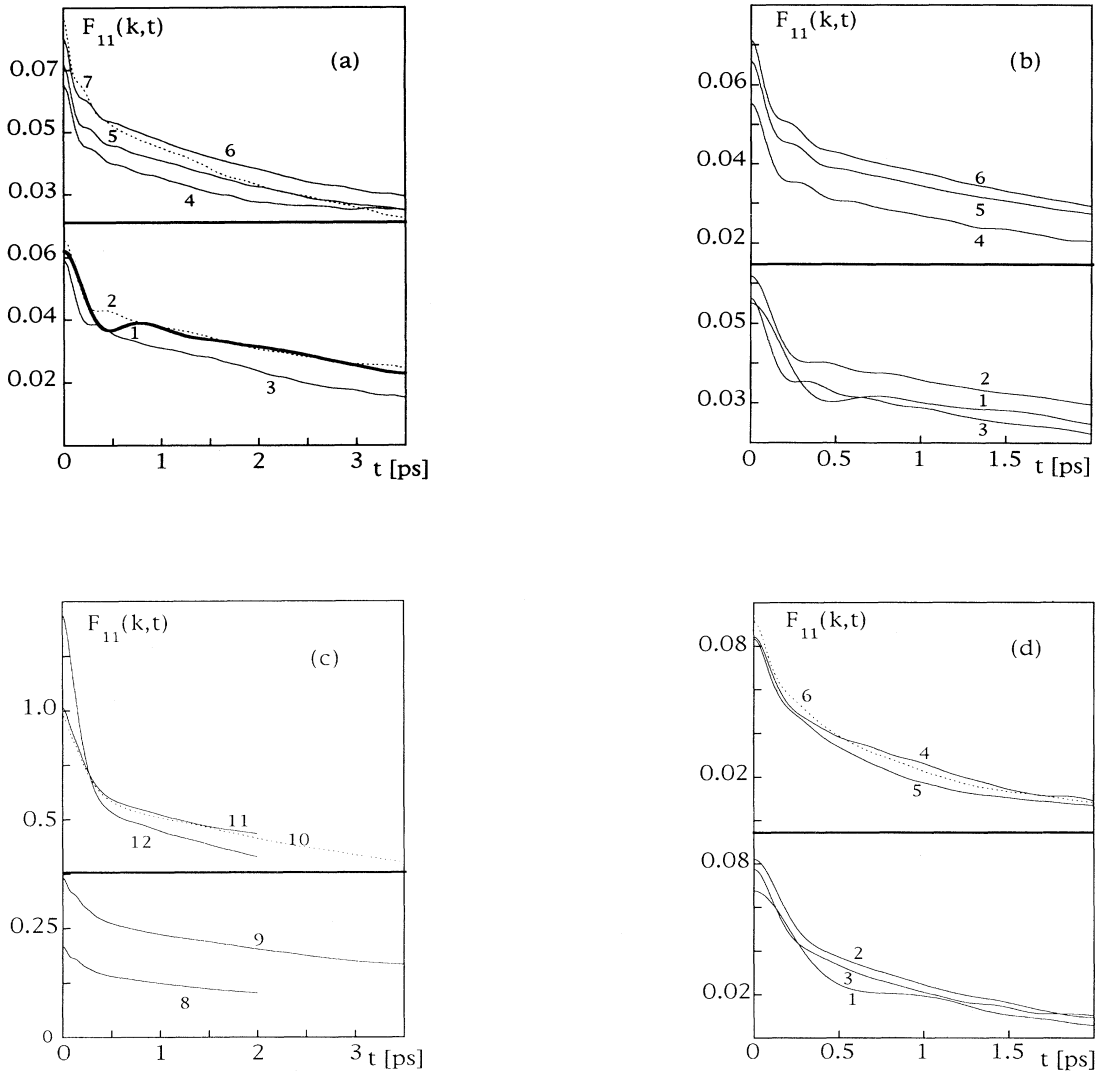

FIG. 1. (a) Density-density ACF at the first seven k values of Table II (run 1, $T=245$ K). (b) Density-density ACF at the first six k values of Table III (run 2, $T=245$ K). (c) Density-density ACF at the other k values of Tables II and III (runs 1 and 2, $T=245$ K). (d) Density-density ACF at the k values of Table IV (run 3, $T=298$ K).

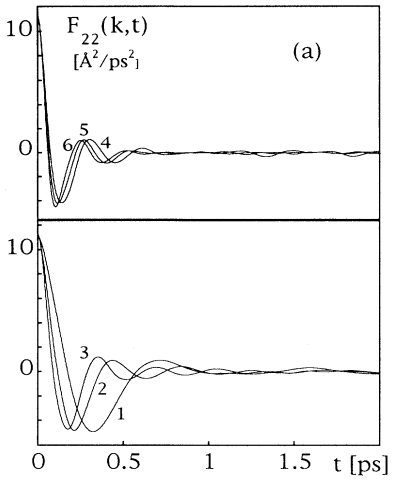

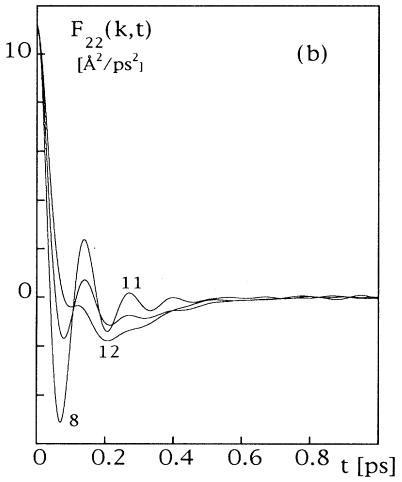

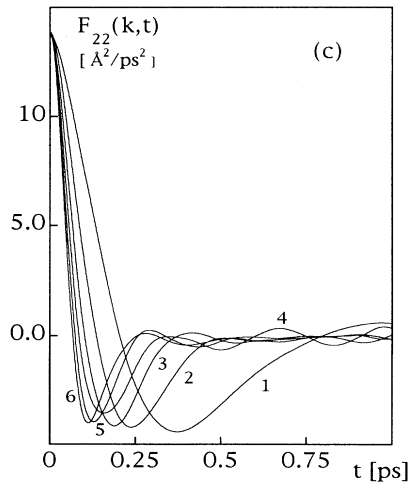

FIG. 2. (a) and (b) Longitudinal current CF's (run 2, $T=245$ K). (c) Longitudinal current CF's (run 3, $T=298$ K).

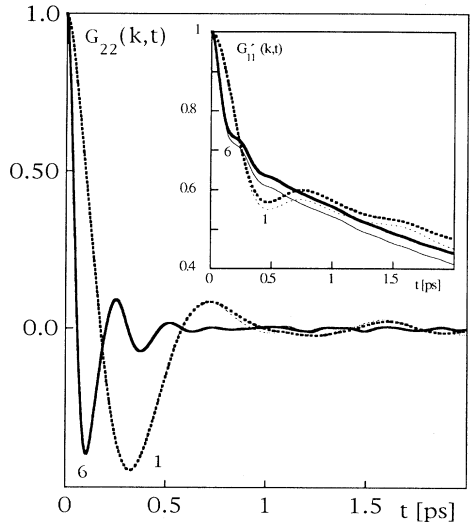

FIG. 3. Normalized longitudinal current ACF at $k=0.288$ and 0.705 Å^{-1}. The inset shows the corresponding density-density ACF. The bold curves are values averaged over runs 1 and 2, while the thin curves relate to run 2.

tional motions, can be seen only in $F_{33}(k,t)$. To make the behavior of this function more consistent with that of all other correlation functions we calculate, the short-time oscillation has been eliminated by extrapolating to $t=0$ a polynomial fit of $F_{33}(k,t)$ vs t^2 (see Fig. 6) in the range 0.06–0.3 ps. The spectrum of the difference between the fitted and the computed function is significantly different from zero only in a frequency range typical of librational motions, with no intensity in the range 0–50 THz. The initial values $V_{ij}(k)$ of the computed time correlation functions are collected in Tables II–IV.

A. Generalized hydrodynamic variables

The generalized thermodynamic variables $h(k)$, $c_v(k)$, $\gamma(k)$, and $\alpha(k)$ calculated according to Eqs. (3.10)–(3.14) and the generalized frequencies $f_{un}(k)$, $f_{u\sigma}(k)$, $f_{uT}(k)$, and $f_{Tq}(k)$ of matrix (3.21) are collected in Table V. The k dependence of $V_{11}(k)\equiv S(k)$ is shown in Fig. 7 at 245

TABLE II. Equal time values of the CF's of run 1 ($T=245$ K).

No.	k (Å^{-1})	V_{11}	V_{22} (Å/ps)^2	$C_l(k,0)$ (Å/ps)^2
1	0.2877	0.0621	11.44	11.42
2	0.4068	0.0656	11.41	11.32
3	0.4982	0.0594	11.36	11.29
4	0.5753	0.0655	11.15	11.44
5	0.6432	0.0720	11.40	11.27
6	0.7046	0.0808	11.34	11.40
7	0.8631	0.0863		
9	1.4668	0.3675		
10	2.0341	0.9785		

TABLE III. Equal time values of the CF's of run 2 ($T=245$ K). In the second part of this table, the energy values used in the CF include a rotational term. $V_{33}^{(c)}$ is the initial value obtained when the librational contribution in $F_{33}(k,t)$ has been removed (see text).

No.	k (Å^{-1})	V_{11}	V_{22} (Å/ps)^2	V_{13} (kJ/mol)	V_{33} (kJ/mol)^2	$V_{33}^{(c)}$ (kJ/mol)^2
1	0.2877	0.0550	11.06	−2.365	145.53	140.17
2	0.4068	0.0618	11.11	−2.660	152.43	145.82
3	0.4982	0.0562	11.29	−2.484	152.69	146.04
4	0.5753	0.0553	11.04	−2.557	143.48	137.99
5	0.6432	0.0658	11.30	−2.890	164.3	157.49
6	0.7046	0.0710	11.36	−3.140	177.59	170.48
8	1.2865	0.209	11.18	−8.848	411.67	403.93
11	2.0744	1.016	11.22	−41.231	1704.3	1693.9
12	2.8766	1.439	11.10	−59.681	2508.7	2494.0
1	0.2877			−2.1311	135.76	134.13
2	0.4068			−2.391	139.12	136.21
3	0.4982			−2.2382	141.64	137.56
4	0.5753			−2.2863	131.79	126.83
5	0.6432			−2.6011	149.31	144.13
6	0.7046			−2.8412	161.10	155.23

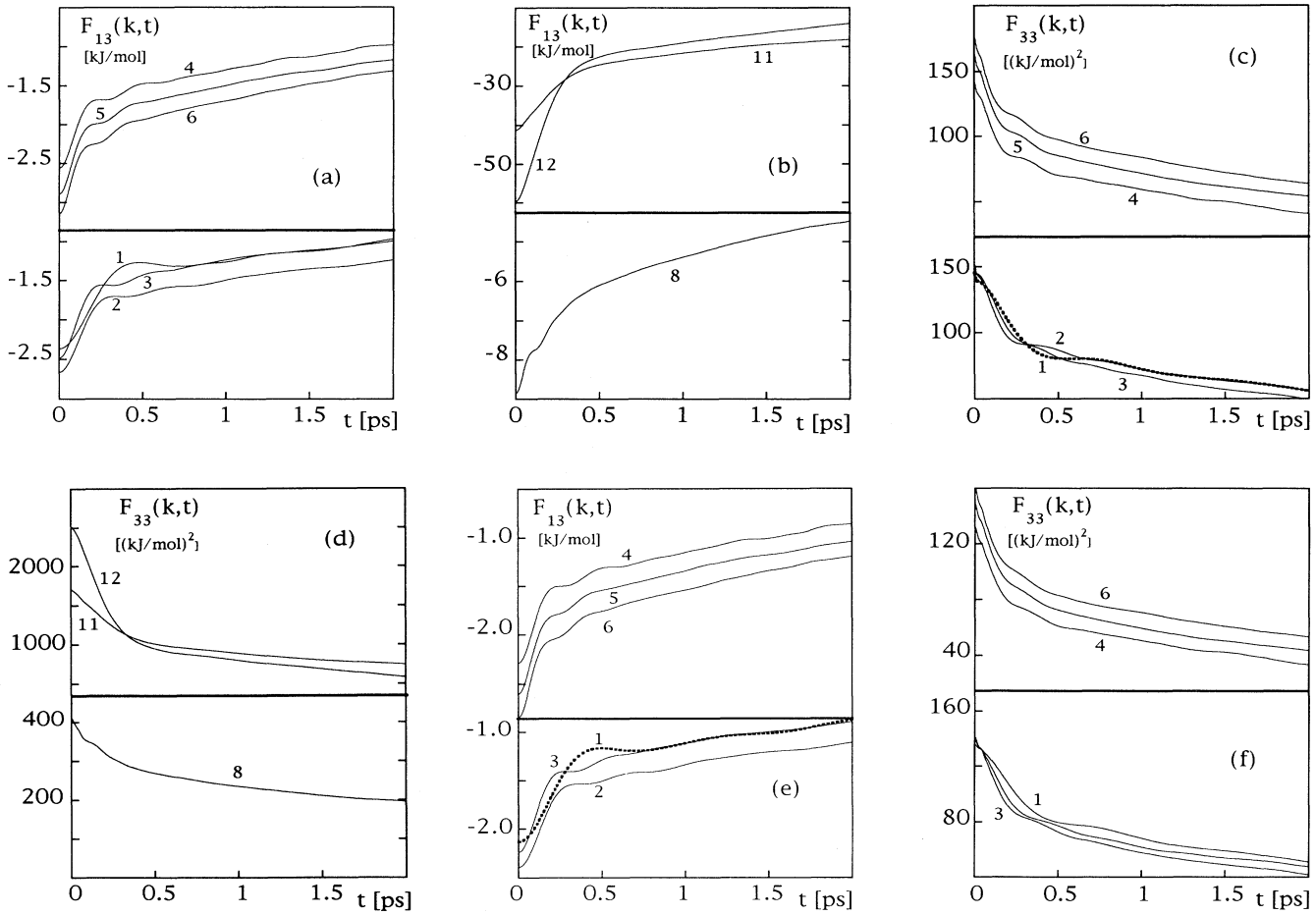

FIG. 4. (a) and (b) Density-energy CF's (run 2, $T=245$ K). (c) and (d) Energy-energy CF's (run 2, $T=245$ K). (e) Density-energy CF's and (f) energy-energy CF's at the k values given in the second part of Table III. The energy values include a rotational kinetic term (see text).

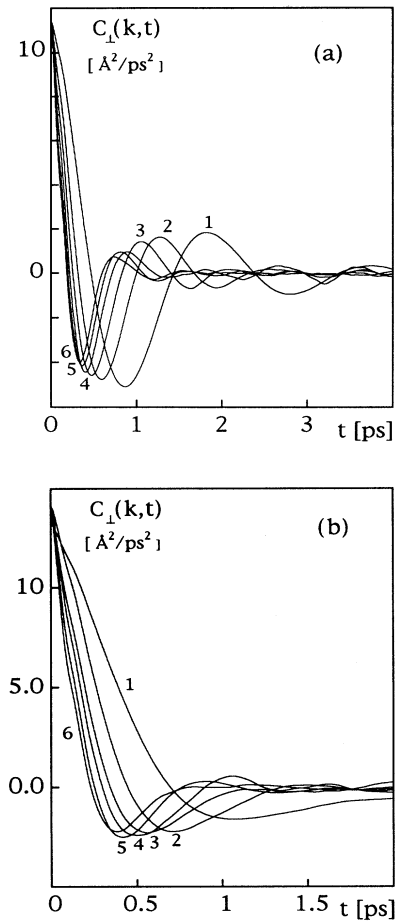

FIG. 5. (a) Transverse current CF's at the first six k values of Table II (run 1, $T=245$ K). (b) Transverse current CF's at the k values of Table IV (run 3, $T=298$ K).

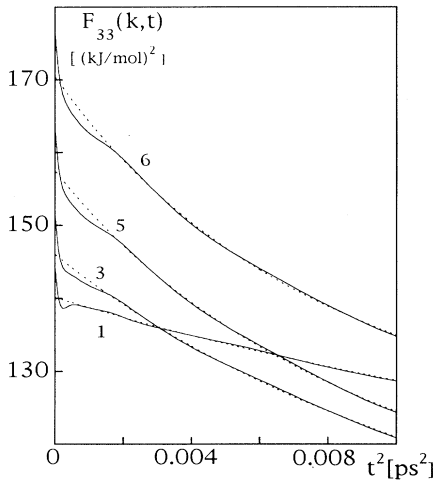

FIG. 6. Enlarged view of the short-time behavior of the energy-energy CF at various k values, with the polynomial representation used to remove the librational glitch (see text). The curves are labeled according to the value of k, reported in Table V.

TABLE IV. Equal time values of the ACF's of run 3 ($T=298$ K).

No.	k (Å^{-1})	V_{11}	V_{22} (Å/ps)^2	$C_\perp(k,0)$ (Å/ps)^2
1	0.2875	0.0676	13.67	13.20
2	0.4066	0.0821	13.87	14.08
3	0.4979	0.0775	13.80	13.59
4	0.5750	0.0843	13.85	14.11
5	0.6428	0.0834	13.80	13.85
6	0.7042	0.0914	13.84	13.67

and 298 K, with a detailed view of the low-k region in the inset, and compared with experimental data from x-ray scattering [39] at 253 and 298 K and at 250 K [40].

As can be seen, the experimental curve lies systematically below the simulation results. Clearly, the main effect of lowering temperature on $S(k)$ is the resolution of the low-k shoulder that becomes a clear peak at 2 Å^{-1}, as a consequence of an enhanced intermediate-range order.

At still smaller k, one can also observe, especially in the low-temperature experimental data, a rising of the $S(k)$ curve to reach the $k=0$ value, computed from the experimental value of the isothermal compressibility. Again, this reflects enhanced correlated density fluctua-

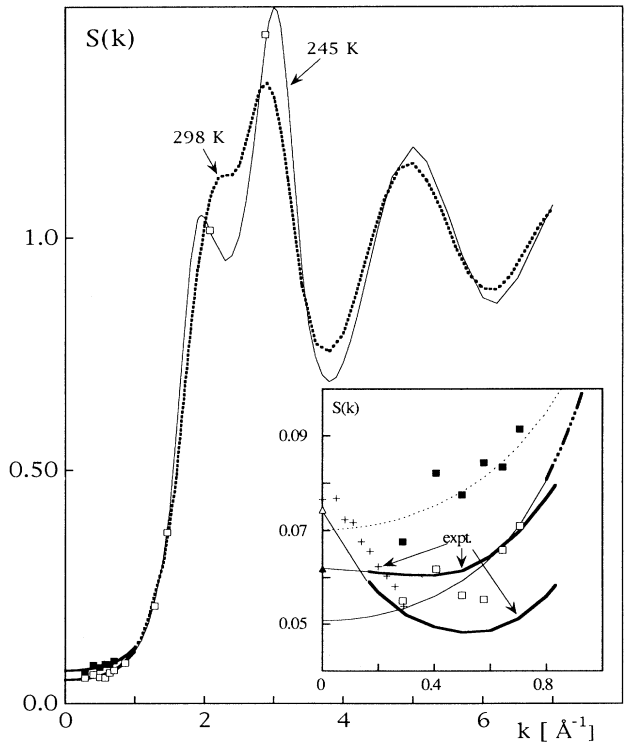

FIG. 7. Comparison of $S(k)$ at 245 and 298 K. The curves are the Fourier transforms of the corresponding radial distribution functions, while the open and solid squares are values obtained as equal time values of the density-density ACF of Tables II–IV. In the inset, the low-k MD results are compared with the experimental x-ray scattering data at 298 and 253 K [39] and at 250 K (crosses) [40].

TABLE V. Generalized thermodynamic properties and frequencies (run 2). The zero-k values are extrapolated data. The second part results have been obtained from initial values of CF's that include a rotational energy term.

No.	k (Å^{-1})	$h(k)$ (kJ/mol)	$c_v(k)$ (J/mol K)	γ (k)	$\alpha(k)$ (10^{-4}/K)	$f_{un}(k)$ (THz)	$f_{u\sigma}(k)$ (THz)	$f_{uT}(k)$ (THz)	$f_{Tq}(k)$ (THz)
0	0	−44.24	87.8	1.0047	−2.0	0	0	0	0
1	0.2877	−44.09	77.3	1.0018	−1.23	4.079	14.01	0.1717	5.45
2	0.4068	−43.52	62.8	1.0005	−0.605	5.453	19.33	0.1183	6.75
3	0.4982	−43.16	72.6	1.0017	1.19	7.064	23.08	0.2934	7.95
4	0.5753	−42.48	39.4	1.0402	4.19	8.131	26.37	1.6309	12.69
5	0.6432	−41.90	61.0	1.0091	2.7	8.432	28.93	0.8022	10.85
6	0.7046	−40.74	63.5	1.0269	4.93	8.912	31.22	1.4629	11.26
8	1.2865	−35.42	60.0	1.3274	28.7	9.401	44.63	5.379	17.78
11	2.0744	−39.24	41.4	1.0884	27.3	6.892	39.94	1.935	19.1
12	2.8766	−38.83	36.2	1.583	76.6	7.992	33.67	5.142	18.4
0	0	−37.5	112	1.0016	1.34	0	0	0	0
1	0.2877	−35.8	103.37	1.0092	3.23	4.079	14.006	0.3903	5.88
2	0.4068	−35.15	87.63	1.0176	4.37	5.453	19.32	0.7244	8.38
3	0.4982	−33.17	96.97	1.0515	7.5	7.064	23.03	1.604	9.84
4	0.5753	−32.83	64.66	1.1245	9.44	8.131	26.27	2.869	13.3
5	0.6432	−31.65	82.71	1.0993	10.4	8.432	28.82	2.657	13.4
6	0.7046	−31.37	83.31	1.1272	12.28	8.912	31.09	3.1786	14.0

tions in the supercooled liquid. According to Xie *et al.* [40], these increased density fluctuations should be associated with a larger fraction of water molecules participating in clusters rather than with increased correlation lengths. This phenomenon is much less apparent in the simulation data, which are also hard to extrapolate reliably at $k=0$, as the isothermal compressibility computed in simulations is affected by a large uncertainty [28].

The k dependence of the generalized thermodynamic properties and frequencies of Table V is shown in Fig. 8. As to $V_{33}(k)$, the equal time value of the energy-energy time correlation function, we have used a "corrected"

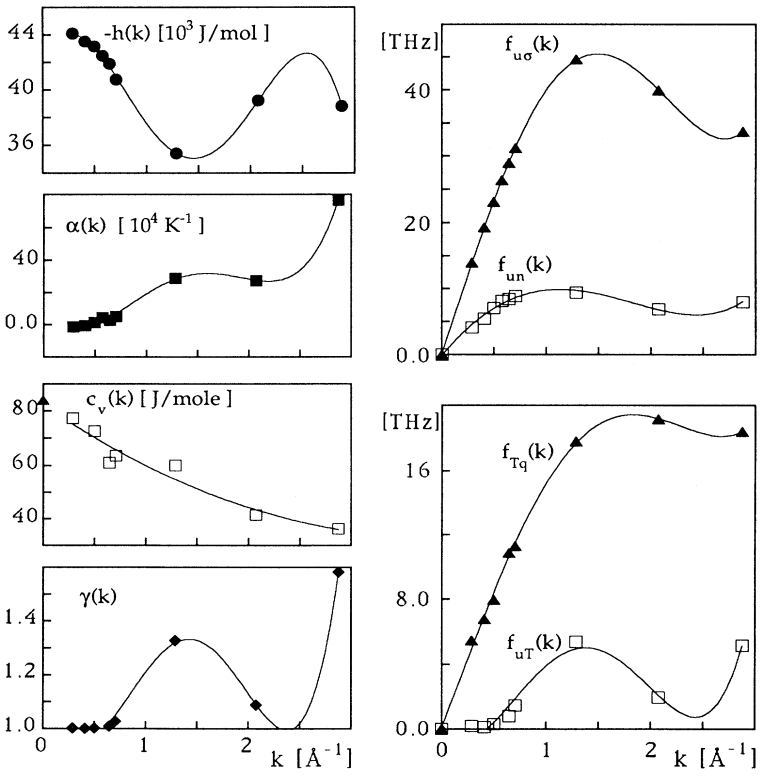

FIG. 8. k dependence of the generalized thermodynamic properties and generalized frequencies. The zero-k value of c_v has been obtained in an independent calculation [24].

value $V_{33}^{(c)}(k)$, where the librational contribution has been removed, as outlined before.

Comparing these results with the corresponding ones for argon [17], one can observe significant differences. Besides the behavior of $S(k)$, two separate peaks at 2 and 3 Å^{-1} for supercooled water, as opposed to one for argon, $h(k)$ is negative at all k's considered and also $\alpha(k)$ becomes negative when $k \to 0$. [The value of $\alpha(k)$ extrapolated to $k=0$ is -2.0×10^{-4} K^{-1}.] It should also be noted that the value of $c_v(0)$, obtained with a polynomial extrapolation as the other data in the second row of Table V, agrees very well with that obtained in a previous independent calculation with no approximations [24].

In the supercooled region, the function $\alpha(k)$, which is negative at $k=0$ in agreement with the experiment [41], crosses the zero at $k=0.45$ Å^{-1} so that γ is exactly 1 at $K=0.45$ Å^{-1} and stays very close to 1 up to $k\sim0.8$ Å^{-1}. The temperature dependence of α [28] allows us to assume that $\gamma(k)$ will be close to 1 also at 298 K for the TIP4P model as in real water. As a consequence, $f_{uT}(k)$, which is proportional to $\gamma(k)-1$, turns out to be negligible compared to $f_{un}(k)$, $f_{u\sigma}(k)$, and $f_{Tq}(k)$.

A further important difference with respect to argon is that $f_{u\sigma}(k)$ is roughly 3–4 times larger than $f_{un}(k)$. In argon $1.5<\gamma<3$, depending on the thermodynamic state [11,12,17,42], and $f_{u\sigma}(k)$ is larger than $f_{un}(k)$ by 50–80 %. We shall see that these two differences play a fundamental role in determining the behavior of the system as to transport phenomena and especially sound propagation.

It is also worth stressing that if the rotational term is included in the calculation of the energy (see the second part of Table III), $\alpha(k)$ is positive, although $\gamma(k)$ is still very close to 1. Moreover, the values of $c_v(k)$ are incorrect. In particular, the value extrapolated at $k=0$ is too large compared with that of Ref. [24]. In our opinion, this depends on including rotational terms only in the energy, so we chose not to include them in all calculated correlation functions, relying on the complete separation between librational and acoustic modes.

B. Hydrodynamic limit

It is important to compare the classical hydrodynamic theory [14,43] with the present generalized approach in the hydrodynamic regime $k,\omega\to0$. The most apparent difference is the frequency dependence of $z_\sigma(k,z)$, $z_q(k,z)$, and $z_{q\sigma}(k,z)$ and the presence of the term $\Delta(k,z)$. It can be shown that $z_{q\sigma}(k,0)\to0$ with k as well as $f_{un}(k)$, $f_{uT}(k)$, $f_{u\sigma}(k)$, and $f_{Tq}(k)$. Hence $\Delta(k,z)\to0$ as k^3 (see Ref. [17]) and can be neglected, while $z_q(k,0)$ and $z_\sigma(k,0)$ tend to a finite limit. So, when $k,\omega\to0$ the following relations hold:

$$\tilde{G}_{11}(k,Z)=\cfrac{1}{z+\cfrac{(c_s^2k^2/\gamma)}{z+\phi k^2+\cfrac{(\gamma-1)(c_s^2k^2/\gamma)}{z+\gamma D_T k^2}}}, \tag{4.1}$$

$$\tilde{G}_{13}(k,z)=\frac{-(c_s^2k^2/\gamma)(\gamma-1)^{1/2}}{\{(z+\gamma D_T k^2)[z^2+\phi k^2 z+(c_s^2k^2/\gamma)]+(\gamma-1)(c_s^2k^2/\gamma)z\}}, \tag{4.2}$$

$$\tilde{G}_{33}(k,z)=\frac{[z^2+\phi k^2 z+(c_s^2k^2/\gamma)]}{\{(z+\gamma D_T k^2)[z^2+\phi k^2 z+(c_s^2k^2/\gamma)]+(\gamma-1)(c_s^2k^2/\gamma)z\}}, \tag{4.3}$$

$$\tilde{G}_{44}(k,z)=\frac{1}{z+z_\sigma(0,0)}, \tag{4.4}$$

$$\tilde{G}_{55}(k,z)=\frac{1}{z+z_q(0,0)}, \tag{4.5}$$

where

$$c_s=\left[\frac{k_BT\gamma}{mS(0)}\right]^{1/2}, \tag{4.6}$$

$$D_T=\frac{\lambda_T}{nmc_p},\quad \phi=\frac{(\frac{4}{3}\eta+\zeta)}{nm}, \tag{4.7}$$

$$z_\sigma(0,0)=\frac{v_{u\sigma}^2}{\phi},\quad z_q(0,0)=\frac{v_{Tq}^2}{\gamma D_T}. \tag{4.8}$$

c_s is the adiabatic sound velocity, D_T and λ_T are the thermal diffusivity and conductivity, and ϕ, η, and ζ are the total, shear, and bulk viscosity. $v_{u\sigma}$ and v_{Tq} are the limits for $k\to0$ of $f_{u\sigma}(k)/k$ and $f_{Tq}(k)/k$, respectively.

Equation (4.1) is the well known classical hydrodynamic expression for the transform of the density-density time correlation function [43]. It is also worth stressing that, under some assumptions for the solution of the cubic equation [42,43] given by the denominators of Eqs. (4.1)–(4.3), one can obtain the following equations in the time domain, i.e.,

the transforms of Eqs. (4.1)–(4.3) with these hypotheses:

$$G_{11}(k,t)=\frac{(\gamma-1)}{\gamma}e^{-\omega_T t}+\frac{e^{-\omega_2 t}}{\gamma}\left\{\cos(\omega_s t)+\left[\frac{\omega_2+(\gamma-1)\omega_T}{\omega_s}\right]\sin(\omega_s t)\right\}, \tag{4.9}$$

$$G_{13}(k,t)=-\frac{(\gamma-1)^{1/2}}{\gamma}\left\{e^{-\omega_T t}-e^{-\omega_2 t}\left[\cos(\omega_s t)+\frac{(\omega_2-\omega_T)}{\omega_s}\sin(\omega_s t)\right]\right\}, \tag{4.10}$$

$$G_{33}(k,t)=\frac{e^{-\omega_T t}}{\gamma}+\frac{(\gamma-1)e^{-\omega_2 t}}{\gamma}\left\{\cos(\omega_s t)+\left[\frac{\omega_2}{\omega_s}+\frac{\omega_T}{\omega_s(\gamma-1)}\right]\sin(\omega_s t)\right\}, \tag{4.11}$$

where

$$\omega_T=D_T k^2,\quad \omega_2=\Gamma k^2,\quad \omega_s=c_s k\ , \tag{4.12}$$

with Γ the sound attenuation coefficient and

$$\omega_2=\frac{\phi k^2+(\gamma-1)\omega_T}{2}\ . \tag{4.13}$$

In this case, the poles of the denominator of Eqs. (4.1)–(4.3) are

$$z_h=\omega_T,\quad z_+=i\omega_s+\omega_2,\quad z_-=-i\omega_s+\omega_2\ . \tag{4.14}$$

Schoen, Vogelsang, and Hoheisel [42] have used Eq. (4.9) to fit the density-density ACF and obtain $\gamma(k)$ and the three frequencies of (4.12). This procedure does not allow us to distinguish a z dependence of z_σ from an increase of $\gamma(k)$, unless the energy-energy and energy-density time correlating functions are also calculated. If, for example, the Laplace transform of the density-density ACF can be well fitted by an expression like Eq. (4.1),

$$\tilde{G}_{11}(k,z)=\frac{1}{z+\dfrac{f_{un}(k)^2}{z+f_{u\sigma}(k)^2\dfrac{1}{z+\gamma_{1n}(k)}+\dfrac{f_{un}(k)^2[\gamma(k)-1]}{z+\gamma_{2n}(k)}}}=\frac{1}{z+\dfrac{f_{un}(k)^2}{z+f_{u\sigma}(k)^2\dfrac{1}{z+z_\sigma(k,z)}}}\ , \tag{4.15}$$

one can interpret this result in two different ways: (i) γ is larger than 1 and a simple exponential dependence of the generalized viscosity [the term that multiplies $f_{u\sigma}(k)^2$ in Eq. (4.15)] and (ii) $\gamma(k)=1$ and a z dependence of $1/[z+z_\sigma(k,z)]$ such as

$$\left\{\frac{\alpha_n(k)}{z+\gamma_{1n}(k)}+\frac{[1-\alpha_n(k)]}{z+\gamma_{2n}(k)}\right\}$$

$$=\left\{\frac{\alpha_n(k)}{z+\gamma_{1n}(k)}+\frac{f_{un}(k)^2[\gamma(k)-1)]}{f_{u\sigma}(k)^2[z+\gamma_{2n}(k)]}\right\}, \tag{4.16}$$

which corresponds, in the time domain, to the linear combination of two exponentials.

From the left-hand side of Eq. (4.16) one can conclude that z_σ does depend on frequency as follows:

$$z_\sigma(k,z)=\frac{\gamma_{1n}\gamma_{2n}+[\alpha_n\gamma_{1n}+(1-\alpha_n)\gamma_{2n}]z}{z+\alpha_n\gamma_{2n}+(1-\alpha_n)\gamma_{1n}}\ . \tag{4.17}$$

From the right-hand side of Eq. (4.16), conversely, one obtains that $z_\sigma(k)=\gamma_{1n}(k)$ so that

$$\gamma(k)-1=[1-\alpha_n(k)]\frac{f_{u\sigma}(k)^2}{f_{un}(k)^2}\ . \tag{4.18}$$

Moreover, if the decay rate $\gamma_{1n}(k)$ is faster than that of $G_{11}(k,t)$, the latter can be fitted in time with an equation equal to Eq. (4.9), as will be shown in the next subsection. This ambiguity can be resolved by an independent calculation of the coefficients $\gamma(k)$, $f_{un}(k)^2$, and $f_{u\sigma}(k)^2$, i.e., by calculating the energy-density and energy-energy time correlation functions.

C. Calculation of $G_{ml}(k,t)$

The $G_{11}(k,t)$, $G_{13}(k,t)$, and $G_{33}(k,t)$ obtained from Eqs. (3.16)–(3.19), using the initial values $V_{jl}(k)$, are shown in Fig. 9 at $k=0.288$ Å^{-1}. These results show the kind of problems one can have when using the optimized parameters, which derive from the fit to $G_{11}(k,t)$ via Eq. (4.9), to calculate $G_{13}(k,t)$ and $G_{33}(k,t)$ by Eqs. (4.10) and (4.11).

The difference from the corresponding functions calculated from the simulation is apparent and is clear evidence of the ambiguity mentioned in the preceding subsection. Actually, the correct $G_{13}(k,t)$ is always small, as it should be when $\gamma=1$ [see Eq. (4.10)] and $G_{33}(k,t)$ behaves like an exponential [Eq. (4.11)]. Hence the incorrect value $\gamma=2.9$ is a consequence of the formal identity Eq. (4.18) and we must conclude that, as $\gamma(k)\cong 1$, z_σ *does* depend on frequency.

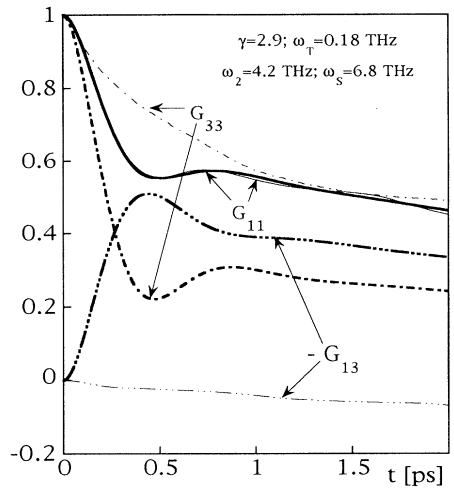

FIG. 9. $G_{11}(k,t)$, $-G_{13}(k,t)$, and $G_{33}(k,t)$ (thin curves), computed from MD data for $k=k_{\min}=0.288$ Å^{-1}. The bold curve labeled $G_{11}(k,t)$ is a fitting function whose optimized parameters have also been used to obtain $G_{13}(k,t)$ and $G_{33}(k,t)$ through Eqs. (4.10) and (4.11).

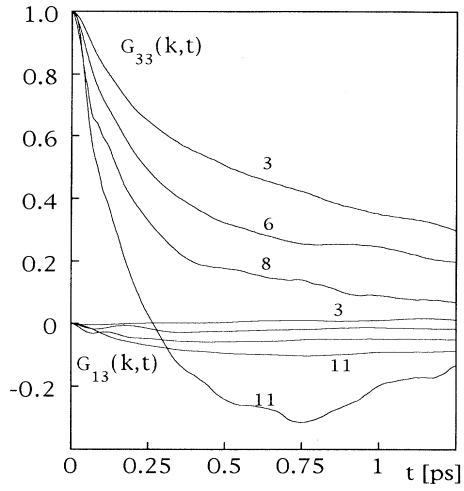

FIG. 10. k dependence of $G_{13}(k,t)$ and $G_{33}(k,t)$ CF's. The curves are labeled according to the value of k given in Table V.

Figure 10 shows our results for $G_{13}(k,t)$ and $G_{33}(k,t)$ at four k values. The amplitude of $G_{13}(k,t)$ is very small at all k up to 1 Å^{-1}, which suggests a simplified approach to the analysis of results. In fact, it can be seen from Eq. (3.24) that $|\tilde{G}_{13}(k,z)|\to 0$ when $f_{uT}(k)\to 0$, i.e., $\gamma\to 1$, and $\Delta(k,z)\to 0$, so that $|z_{q\sigma}(k,z)|\to 0$. As the first condition is fulfilled at least up to 1 Å^{-1}, the second also must be substantially obeyed [note that $z_{q\sigma}(k)$ is close to zero even for argon up to ≈ 2 Å^{-1} [17]].

Under these circumstances, Eqs. (3.23)–(3.27) become

$$\tilde{G}_{11}(k,z)\cong\frac{1}{z+\dfrac{f_{un}(k)^2}{z+\dfrac{f_{u\sigma}(k)^2}{[z+z_\sigma(k,z)]}}}\,, \tag{4.19}$$

$$\tilde{G}_{13}(k,z)\cong 0\,, \tag{4.20}$$

$$\tilde{G}_{33}(k,z)\cong\frac{1}{z+\dfrac{f_{Tq}(k)^2}{[z+z_q(k,z)]}}\,, \tag{4.21}$$

$$\tilde{G}_{44}(k,z)\cong\frac{[z^2+f_{un}(k)^2]}{\{[z+z_\sigma(k,z)]\}\left[z^2+\dfrac{f_{u\sigma}(k)^2}{[z+z_\sigma(k,z)]}z+f_{un}(k)^2\right]}\,, \tag{4.22}$$

$$\tilde{G}_{55}(k,z)\cong\frac{z}{\{[z+z_q(k,z)]\}\left[z+\dfrac{f_{Tq}(k)^2}{[z+z_q(k,z)]}\right]}\,, \tag{4.23}$$

and $\Delta(k,z)\cong 0$. It is worth observing that when $\gamma(k)\cong 1$, $\alpha(k)\cong 0$, and $G_{13}(k,t)\cong 0$, $G_{33}(k,t)$ is equivalent to the temperature-temperature ACF [20,44]. To fit the Laplace transforms of the time correlation function according to Eqs. (4.19)–(4.21) and to obtain the transport coefficients $z_\sigma(k,z)$ and $z_q(k,z)$, it remains to assume a functional dependence of the latter on frequency.

In the following, the models proposed in the literature will be compared with one introduced here to allow a more accurate description of the short-time behavior of these transport coefficients and also to take into account the effects due to single-molecule modes, mainly for k's typical of simulation and neutron scattering experiments (>0.2 Å^{-1}).

V. MODELS FOR THE TRANSPORT COEFFICIENTS

To fit the equations in the frequency domain and obtain the generalized transport coefficients $z_\sigma(k,z)$ and

$z_q(k,z)$, a functional dependence of these coefficients on frequency must be assumed. The relations used for the fit are Eqs. (4.19)–(4.23) in Sec. IV C, valid when, as in the case of water for $k<1$ Å^{-1}, the two conditions $\gamma(k)=c_p(k)/c_v(k)\cong 1$ and $z_{q\sigma}(k)\approx 0$ are fulfilled.

The generalized transport coefficients $z_s(k,z)$ and $z_q(k,z)$ are the transforms of the correlation functions $J_\sigma(k,t)$ and $J_q(k,t)$ [see Eqs. (A18) and (A19) in Ref. [17]] and the latter two CF's are the memory kernel of $n_\sigma(k,t)$ and $n_q(k,t)$:

$$\tilde{n}_\sigma(k,z)=\frac{1}{z+z_\sigma(k,z)} , \tag{5.1}$$

$$\tilde{n}_q(k,z)=\frac{1}{z+z_q(k,z)} . \tag{5.2}$$

The models previously employed in the literature assume an exponential time dependence of $n_\sigma(k,t)$ and $n_q(k,t)$ [19–22] (simple viscoelastic model) or a linear combination of two exponentials for $n_\sigma(k,t)$ [12]. In the latter case, which will be referred to as model n in the following, one has

$$n_\sigma(k,t)=[1-\alpha_n^{(\sigma)}(k)]e^{-\gamma_{1n}^{(\sigma)}(k)t}+\alpha_n^{(\sigma)}(k)e^{-\gamma_{2n}^{(\sigma)}(k)t} . \tag{5.3}$$

General arguments [10,18,45] lead us to conclude that the time derivative of $n_\sigma(k,t)$ and $n_q(k,t)$ must vanish at $t=0$, a constraint obviously violated by the simple viscoelastic model and by model n. Furthermore, while the viscoelastic model assumes that z_σ depends just on k, model n leads to a k and a z dependence of z_σ [see Eq. (5.1) and the transform of Eq. (5.3)] such as

$$z_\sigma(k,z)=\frac{a_{1n}^{(\sigma)}(k)z+a_{0n}^{(\sigma)}(k)}{z+b_{0n}^{(\sigma)}(k)} , \tag{5.4}$$

where

$$\begin{aligned} a_{0n}^{(\sigma)}(k)&=\gamma_{1n}^{(\sigma)}(k)\gamma_{2n}^{(\sigma)}(k) , \\ a_{1n}^{(\sigma)}(k)&=[1-\alpha_n^{(\sigma)}(k)]\gamma_{1n}^{(\sigma)}(k)+\alpha_n^{(\sigma)}(k)\gamma_{2n}^{(\sigma)}(k) , \\ b_{0n}^{(\sigma)}(k)&=[1-\alpha_n^{(\sigma)}(k)]\gamma_{2n}^{(\sigma)}(k)+\alpha_n^{(\sigma)}(k)\gamma_{1n}^{(\sigma)}(k) . \end{aligned} \tag{5.5}$$

In both cases, the short-time behavior of $J_\sigma(k,t)$ and $J_q(k,t)$, i.e., the Laplace transforms of $z_\sigma(k,z)$ and $z_q(k,z)$, is described incorrectly. In fact, the viscoelastic treatment assumes a complete time scale separation between the relaxation time of $G_{11}(k,t)$ and $J_\sigma(k,t)$, so that z_σ takes the zero-frequency value, while model n implicitly assumes a fast decay of the correlation function, whose contribution is $a_{1n}^{(\sigma)}(k)$, i.e., $z\to\infty$ in Eq. (5.4).

In the case of water, the viscoelastic model cannot be adopted, in view of the frequency dependence of $z_\sigma(k,z)$ and $z_q(k,z)$. Moreover, it is necessary to include in the description both the collective acoustic mode and single-molecule modes, especially the one corresponding to the 45-THz band in the spectrum of the center of mass velocity ACF. All this stresses the importance of a good description of the short-time part of $n_\sigma(k,t)$ and $n_q(k,t)$.

It is more convenient to set up a model for $J_\sigma(k,t)$ and $J_q(k,t)$ rather than $n_\sigma(k,t)$ and $n_q(k,t)$, so the new model will be labeled model J. To make sure that the latter correlation functions have the correct short-time behavior keeping two well separated time scales, we chose a time dependence of the form

$$\begin{aligned} \frac{J_\sigma(k,t)}{J_\sigma(k,0)}&=\alpha_J^{(\sigma)}(k)e^{-\gamma_{1J}^{(\sigma)}(k)t} \\ &\times\left[\cos[\omega_J^{(\sigma)}(k)t]+m_J^{(\sigma)}(k)\frac{\sin[\omega_J^{(\sigma)}(k)t]}{\omega_J^{(\sigma)}(k)}\right] \\ &+[1-\alpha_J^{(\sigma)}(k)]e^{-\gamma_{2J}^{(\sigma)}(k)t} , \end{aligned} \tag{5.6}$$

where

$$m_J^{(\sigma)}(k)=\gamma_{1J}^{(\sigma)}(k)+\frac{[1-\alpha_J^{(\sigma)}(k)]}{\alpha_J^{(\sigma)}(k)}\gamma_{2J}^{(\sigma)}(k) . \tag{5.7}$$

Relations (5.6) and (5.7) describe a z dependence of $z_\sigma(k,z)$ such as

$$\frac{z_\sigma(k,z)}{J_\sigma(k,0)}=\frac{z^2+a_{1J}^{(\sigma)}(k)z+a_{0J}^{(\sigma)}(k)}{z^3+a_{1J}^{(\sigma)}(k)z^2+b_{1J}^{(\sigma)}(k)z+b_{0J}^{(\sigma)}(k)} , \tag{5.8}$$

where

$$\begin{aligned} a_{1J}^{(\sigma)}&=2\gamma_{1J}^{(\sigma)}+\gamma_{2J}^{(\sigma)} , \\ a_{0J}^{(\sigma)}&=2\gamma_{1J}^{(\sigma)}\gamma_{2J}^{(\sigma)}\alpha_J^{(\sigma)} \\ &\quad+(1-\alpha_J^{(\sigma)})(\gamma_{1J}^{(\sigma)2}+\gamma_{2J}^{(\sigma)2}+\omega_J^{(\sigma)2}) , \\ b_{1J}^{(\sigma)}&=\gamma_{1J}^{(\sigma)2}+\omega_J^{(\sigma)2}+2\gamma_{1J}^{(\sigma)}\gamma_{2J}^{(\sigma)} , \\ b_{0J}^{(\sigma)}&=\gamma_{2J}^{(\sigma)}(\gamma_{1J}^{(\sigma)2}+\omega_J^{(\sigma)2}) , \end{aligned} \tag{5.9}$$

and the k dependence has been omitted for simplicity.

The number of parameters increases to 5 from 3 for model n. This is a straightforward consequence of the fact that model J also describes the single-molecule mode at $\sim$45 THz. In fact, the two extra parameters are the frequency and the decay rate of the single-molecule mode. Moreover, model J, besides the correct description of the short-time behavior, allows us to know $J_\sigma(k,t)$, the memory kernel of $n_\sigma(k,t)$. This is not possible with model n as Eq. (5.4) cannot be inverted, unless the $z\to\infty$ limit is subtracted. In this case $J_\sigma(k,t)$ would be an exponential with an amplitude $(a_{0n}^{(\sigma)}-a_{1n}^{(\sigma)}b_{0n}^{(\sigma)})$ and a decay rate $(1/b_{0n}^{(\sigma)})$.

Equations (5.6)–(5.9) can also be applied to $J_q(k,t)$, $z_q(k,z)$, and $n_q(k,t)$, with the parameter index changing from σ to q. For model n we have

$$G_{11}(k,\omega)=\frac{f_{u\sigma}^2 f_{un}^2(a_{0n}^{(\sigma)}b_{0n}^{(\sigma)}+\omega^2 a_{1n}^{(\sigma)})}{C_{1n}^2+\omega^2 D_{1n}^2} , \tag{5.10}$$

where

$$C_{1n}=\omega^4-\omega^2(a_{0n}^{(\sigma)}+f_{un}^2+f_{u\sigma}^2)+a_{1n}^{(\sigma)}f_{un}^2 \tag{5.11}$$

and

$$D_{1n}=b_{0n}^{(\sigma)}f_{u\sigma}^2+(a_{1n}^{(\sigma)}+b_{0n}^{(\sigma)})(f_{un}^2-\omega^2) . \tag{5.12}$$

The Laplace transform of $G_{33}(k,t)$, the real part, is

$$G_{33}(k,\omega)=\frac{f_{Tq}^2(a_{0n}^{(q)}b_{0n}^{(q)}+\omega^2 a_{1n}^{(q)})}{\{[b_{0n}^{(q)}f_{Tq}^2-\omega^2(a_{1n}^{(q)}+b_{0n}^{(q)})]^2+\omega^2[\omega^2-(a_{0n}^{(q)}+f_{Tq}^2)]^2\}} . \tag{5.13}$$

The same relations with model J become

$$G_{11}(k,\omega)=\frac{f_{u\sigma}^2 f_{un}^2 J_\sigma[a_{0J}^{(\sigma)}b_{0J}^{(\sigma)}+\omega^2(a_{1J}^{(\sigma)}b_{1J}^{(\sigma)}-a_{0J}^{(\sigma)}a_{1J}^{(\sigma)}-b_{0J}^{(\sigma)})]}{C_{1J}^2+\omega^2 D_{1J}^2} , \tag{5.14}$$

where

$$C_{1J}=\omega^6-\omega^4(J_\sigma+b_{1J}^{(\sigma)}+f_{un}^2+f_{u\sigma}^2)+\omega^2[J_\sigma a_{0J}^{(\sigma)}+f_{u\sigma}^2 b_{1J}^{(\sigma)}+f_{un}^2(J_\sigma+b_{1J}^{(\sigma)})]-f_{un}^2 J_\sigma a_{0J}^{(\sigma)} \tag{5.15}$$

and

$$D_{1J}=a_{1J}^{(1)}\omega^4-\omega^2[b_{0J}^{(\sigma)}+a_{1J}^{(\sigma)}(J_\sigma+f_{un}^2+f_{u\sigma}^2)]+f_{u\sigma}^2 b_{0J}^{(\sigma)}+f_{un}^2(b_{0J}^{(\sigma)}+J_\sigma a_{1J}^{(\sigma)}) \tag{5.16}$$

and, for the transform of $G_{33}(k,t)$,

$$G_{33}(k,\omega)=\frac{f_{Tq}^2 J_q[a_{0J}^{(q)}b_{0J}^{(q)}+\omega^2(a_{1J}^{(q)}b_{1J}^{(q)}-a_{0J}^{(q)}a_{1J}^{(q)}-b_{0J}^{(q)})]}{C_{3J}^2+\omega^2 D_{3J}^2} , \tag{5.17}$$

where

$$C_{3J}=a_{1J}^{(q)}\omega^4-\omega^2[b_{0J}^{(q)}+a_{1J}^{(q)}(J_q+f_{Tq}^2)]+b_{0J}^{(q)}f_{Tq}^2 \tag{5.18}$$

and

$$D_{3J}=\omega^4-\omega^2(b_{1J}^{(q)}+J_q+f_{Tq}^2)+a_{0J}^{(q)}J_q+b_{1J}^{(q)}f_{Tq}^2 . \tag{5.19}$$

In Eqs. (5.14)–(5.19) the k dependence has been omitted for simplicity and $J_\sigma\equiv J_\sigma(k,0)$ and $J_q\equiv J_q(k,0)$.

For a correct comparison of models n and J, the time dependence of $n_\sigma(k,t)$, which corresponds to the time dependence of $J_\sigma(k,t)$ as given by model J [Eq. (5.6)], can be calculated. Inverting Eq. (5.1) and using Eq. (5.8), it can be shown that the corresponding time correlation function is of the form

$$n_\sigma(k,t)=[1-\alpha_{1n}^{(\sigma J)}(k)-\alpha_{2n}^{(\sigma J)}(k)]e^{-\gamma_{3n}^{(\sigma J)}(k)t}\left[\cos[\omega_n^{(\sigma J)}(k)t]+m_n^{(\sigma)}(k)\frac{\sin[\omega_n^{(\sigma J)}(k)t]}{\omega_n^{(\sigma J)}(k)}\right]$$
$$+\alpha_{1n}^{(\sigma J)}(k)e^{-\gamma_{1n}^{(\sigma J)}(k)t}+\alpha_{2n}^{(\sigma J)}(k)e^{-\gamma_{2n}^{(\sigma J)}(k)t} , \tag{5.20}$$

where

$$m_n^{(\sigma)}(k)=\frac{\alpha_{1n}^{(\sigma J)}(k)\gamma_{1n}^{(\sigma J)}(k)+\alpha_{2n}^{(\sigma J)}(k)\gamma_{2n}^{(\sigma J)}(k)+[1-\alpha_{1n}^{(\sigma J)}(k)-\alpha_{2n}^{(\sigma J)}(k)]\gamma_{3n}^{(\sigma J)}(k)}{[1-\alpha_{1n}^{(\sigma J)}(k)-\alpha_{2n}^{(\sigma J)}(k)]} . \tag{5.21}$$

In Eqs. (5.20) and (5.21) the index (σJ) relates to coefficients obtained from model J. In the Appendix, the method used to calculate these coefficients, from those of Eqs. (5.6) and (5.7), is described in detail.

Moreover, from Eqs. (5.6), (5.7), (5.20), and (5.21), we obtain

$$\begin{aligned}&\dot{n}_\sigma(k,0)=0 ,\\ &\ddot{n}_\sigma(k,0)=-J_\sigma ,\\ &\dddot{n}_\sigma(k,0)=0 ,\\ &\ddddot{n}_\sigma(k,0)=J_\sigma^2+[b_{1J}^{(\sigma)}(k)-a_{0J}^{(\sigma)}(k)]J_\sigma .\end{aligned} \tag{5.22}$$

Comparing Eqs. (5.22) with the correct short-time behavior of $n_\sigma(k,t)$ [10,18]

$$n_\sigma(k,t)=\mathrm{sech}^2[t/\tau_c(k)] , \tag{5.23}$$

we get, from the second of Eqs. (5.22),

$$\tau_c(k)=\left[\frac{2}{J_\sigma}\right]^{1/2} . \tag{5.24}$$

On the other hand, the fourth time derivative term would be, according to Eq. (5.23),

$$\ddddot{n}_\sigma(k,0)=\frac{16}{\tau_c^4(k)}=4J_\sigma^2 . \tag{5.25}$$

This result, though not exact, is very close to that one obtains from Eq. (5.24) and the fourth of Eqs. (5.22). All these considerations show that J_σ is simply related to the collision time τ_c [10,18,45].

VI. FIT OF THE TRANSFORMED CF'S AND SOUND DISPERSION

The optimized parameters obtained from a fit to the Laplace transforms of the density-density ACF according to models J and n are collected in Tables VI–IX at

TABLE VI. (a) Computed (c) and optimized generalized frequencies and parameters used to fit $G_{11}(k,\omega)$ with model J [Eq. (5.14)]. (b) Coefficients required to compute $n_\sigma(k,t)$ according to Eq. (5.20). These values have been obtained from (a) as described in the Appendix ($T=245$ K).

No.	k (Å^{-1})	$[f^2_{un}]_{fJ}$ (THz)^2	$[f^2_{un}]_c$ (THz)^2	$[f^2_{u\sigma}]_{fJ}$ (THz)^2	$[f^2_{u\sigma}]_c$ (THz)^2	J_σ (THz)^2	$\gamma^{(\sigma)}_{1J}$ (THz)	$\gamma^{(\sigma)}_{2J}$ (THz)	$\omega^{(\sigma)}_J$ (THz)	$a^{(\sigma)}_J$
					(a)					
1	0.2877	16.94	17.3	165.8	196.3	953.7	16.8	3.44	42.8	1.0485
2	0.4067	29.53	29.5	319.2	373.6	907.5	16.7	2.79	43.5	1.0357
3	0.4983	49.85	51.0	443.7	532.7	831.6	16.9	2.76	41.5	1.0370
4	0.5754	65.06	66.5	562.4	695.4	765.6	17.3	2.39	40.1	1.0331
5	0.6432	69.96	71.0	696.3	837	796.0	19.1	2.26	41.7	1.0322
6	0.7046	77.48	79.4	801.0	974.7	765.6	19.9	2.33	41.9	1.0330
7	0.8631	94.81	97.3	1105	1274	790.6	24.4	2.16	43.4	1.0316

No.	k (Å^{-1})	$\gamma^{(\sigma J)}_{1n}$ (THz)	$\gamma^{(\sigma J)}_{2n}$ (THz)	$\gamma^{(\sigma J)}_{3n}$ (THz)	$\omega^{(\sigma J)}_n$ (THz)	$\alpha^{(\sigma J)}_{1n}$	$\alpha^{(\sigma J)}_{2n}$
				(b)			
1	0.2877	14.49	0.414	11.07	52.22	0.5273	0.1590
2	0.4067	13.10	0.459	11.32	52.26	0.5682	0.1398
3	0.4983	13.15	0.530	11.44	49.83	0.5757	0.1350
4	0.5754	12.90	0.532	11.78	47.92	0.6031	0.1171
5	0.6432	13.52	0.470	13.18	49.37	0.6331	0.1047
6	0.7046	13.69	0.523	13.94	49.11	0.6421	0.1126
7	0.8631	15.61	0.543	17.37	50.02	0.6988	0.0943

TABLE VII. Same as Table VI (a) for model n [Eq. (5.10)]. The last three columns report the time integral of the memory kernel of the models and of the normalized density-density ACF.

No.	k (Å^{-1})	$[f^2_{un}]_{fn}$ (THz)^2	$[f^2_{u\sigma}]_{fn}$ (THz)^2	$\gamma^{(\sigma)}_{1n}$ (THz)	$\gamma^{(\sigma)}_{2n}$ (THz)	$\alpha^{(\sigma)}_n$	$[n_\sigma(k,0)]_{fn}$ (ps)	$[n_\sigma(k,0)]_{fJ}$ (ps)	$G_{11}(k,0)$ (ps)
1	0.2877	16.5	139.2	17.4	0.428	0.191	0.4927	0.4257	4.17
2	0.4067	28.1	271.5	16.7	0.505	0.174	0.3940	0.3531	3.78
3	0.4983	47.0	411.8	20.4	0.723	0.187	0.2985	0.3040	2.65
4	0.5754	61.7	565.1	22.8	0.765	0.163	0.2498	0.2728	2.29
5	0.6432	67.1	753.0	25.6	0.679	0.147	0.2498	0.2863	2.80
6	0.7046	76.1	938.5	27.9	0.758	0.144	0.2206	0.2685	2.72
7	0.8631	98.0	1515	32.0	0.777	0.107	0.1656	0.2250	2.57

TABLE VIII. Same as Table VI at 298 K.

No.	k (Å^{-1})	$[f^2_{un}]_{fJ}$ (THz)^2	$[f^2_{un}]_c$ (THz)^2	$[f^2_{u\sigma}]_{fJ}$ (THz)^2	$[f^2_{u\sigma}]_c$ (THz)^2	J_σ (THz)^2	$\gamma^{(\sigma)}_{1J}$ (THz)	$\gamma^{(\sigma)}_{2J}$ (THz)	$\omega^{(\sigma)}_J$ (THz)	$\alpha^{(\sigma)}_J$
1	0.2875	17.3	17.3	152.9	170	1391	36.0	4.18	55.0	1.0390
2	0.4066	28.1	28.2	294.0	342	1275	29.0	3.86	51.1	1.0316
3	0.4979	45.6	44.4	445.1	490	1261	37.1	4.27	51.4	1.0409
4	0.5750	53.4	52.5	560.7	640	1250	33.8	4.48	48.6	1.0488
5	0.6428	68.4	68.5	662.8	778	1206	37.1	6.32	50.2	1.0441
6	0.7041	74.1	74.6	761.1	900	1195	40.7	5.77	48.5	1.0546

No.	k (Å^{-1})	$\gamma^{(\sigma J)}_{1n}$ (THz)	$\gamma^{(\sigma J)}_{2n}$ (THz)	$\gamma^{(\sigma J)}_{3n}$ (THz)	$\omega^{(\sigma J)}_n$ (THz)	$\alpha^{(\sigma J)}_{1n}$	$\alpha^{(\sigma J)}_{2n}$
1	0.2875	24.42	1.755	25.06	63.52	0.6994	0.0982
2	0.4066	20.66	1.863	19.67	60.34	0.6581	0.0900
3	0.4979	25.38	1.969	25.56	59.15	0.7174	0.0940
4	0.5750	25.54	1.886	22.38	57.30	0.6569	0.1002
5	0.6428	25.63	3.735	25.55	57.67	0.7043	0.1131
6	0.7041	29.19	2.944	27.56	55.36	0.7241	0.1111

TABLE IX. Same as Table VII at 298 K.

No.	k (Å^{-1})	$[f^2_{un}]_{fn}$ (THz)^2	$[f^2_{u\sigma}]_{fn}$ (THz)^2	$\gamma^{(\sigma)}_{1n}$ (THz)	$\gamma^{(\sigma)}_{2n}$ (THz)	$\alpha^{(\sigma)}_n$	$[n_\sigma(k,0)]_{fn}$ (ps)	$[n_\sigma(k,0)]_{fJ}$ (ps)	$G_{11}(k,0)$ (ps)
1	0.2875	17.2	216.2	41.1	1.99	0.0878	0.0664	0.0905	0.78
2	0.4066	27.7	306.7	26.9	2.10	0.0970	0.0797	0.0861	0.85
3	0.4979	45.6	566.5	35.65	2.39	0.0876	0.0624	0.0828	0.77
4	0.5750	53.7	774.4	42.18	2.54	0.0933	0.0581	0.0862	0.85
5	0.6428	69.5	942.8	42.98	5.44	0.1270	0.0436	0.0648	0.61
6	0.7041	76.0	1137	43.6	3.52	0.0915	0.0469	0.0706	0.70

$T=245$ and 298 K. In most cases the parameter δ, introduced in Sec. II, is given the value 1 ps^2, to allow us to balance the low- and high-frequency information. In Tables VI–IX, the $f_{un}(k)^2$ have been obtained from the second moment of $G_{11}(k,t)$ and agree with the corresponding data of Table V within the statistical uncertainty. The results for $G_{33}(k,\omega)$ are shown in Tables X and XI.

The spectra calculated from the MD correlation functions and those from the fitting functions are compared in Figs. 11–13 at some values of k. As can be seen, both models reproduce accurately $\omega^2 G_{11}(k,\omega)$ at the smallest k, except that the band at about 45 THz is missing in the fit with model n. The data relevant to model n in Table I at $k>0.5$ Å^{-1} have been obtained with $\delta=1/f_{un}(k)^2$ as those obtained with $\delta=1$ ps^2 are unphysical. This problem does not show up at 298 K as the bands corresponding to single-molecule modes are less resolved and model n is able to compensate by a large increase of $[f_{u\sigma}(k)^2]_f$.

Model J, on the other hand, is only weakly dependent on δ and leads to values of $f_{un}(k)^2$, $f_{u\sigma}(k)^2$, and $f_{Tq}(k)^2$ very close to those calculated independently from $V_{ml}(k)$. Note that although the $[f_{u\sigma}(k)^2]_f$ from model J are systematically underestimated by $\sim 15\%$, their ratio to the correct values does not depend on k.

In the case of $G_{33}(k,\omega)$ (Tables X and XI) model n shows more clearly its limitations, so only results relevant to $k=k_{\min}$ and $3k_{\min}$ are reported. In fact, in this case there are two separate bands and model n cannot compensate the effect of the higher-frequency band by increasing $f_{Tq}(k)^2$. Actually, the main bands of the spectra shown in Fig. 13 are those at 10–15 and 45–60 THz. Their position depends slightly on k, while the amplitude of the high-frequency band increases much more rapidly with k.

It is also worth stressing the different behavior of $J_\sigma(k,t)$ and $J_q(k,t)$. Both correlation functions show a fast decay followed by a long-time tail, but the latter is negative for $J_\sigma(k,t)$ $[1-\alpha_J^{(\sigma)}(k)]<0$ and positive for $J_q(k,t)$ $[1-\alpha_J^{(q)}(k)]>0$. This difference is confirmed by

TABLE X. (a) Computed (c) and optimized generalized frequencies and parameters used to fit $G_{33}(k,\omega)$ with model J [Eq. (5.17)]. (b) Coefficients required to compute $n_q(k,t)$. These values have been obtained from (a) as described in the Appendix ($T=245$ K). The last two columns are the time integral of the temperature-temperature ACF and the corresponding generalized thermal diffusivity [see Eq. (10.2)].

No.	k (Å^{-1})	$[f^2_{Tq}]_{fJ}$ (THz)^2	$[f^2_{Tq}]_c$ (THz)^2	J_q (THz)^2	$\gamma^{(q)}_{1J}$ (THz)	$\gamma^{(q)}_{2J}$ (THz)	$\omega^{(q)}_J$ (THz)	$\alpha^{(q)}_J$
				(a)				
1	0.2877	30.9	29.7	1123.4	41.4	3.05	40.9	0.8997
3	0.4983	74.0	63	1191	25.1	2.26	38.6	0.9047
5	0.6432	153	118	1618	40.5	1.69	41.6	0.9501
6	0.8046	153	127	1525	35.5	1.68	40.3	0.9381
8	1.2865	315	316	2187	50.9	3.58	32.8	0.9747
11	2.0744	257		1125	30.81	4.08	33.0	1.0867
12	2.8766	251		983	25.4	7.27	39.8	0.9891

No.	k (Å^{-1})	$\gamma^{(qJ)}_{1n}$ (THz)	$\gamma^{(qJ)}_{2n}$ (THz)	$\gamma^{(qJ)}_{3n}$ (THz)	$\omega^{(qJ)}_n$ (THz)	$\alpha^{(qJ)}_{1n}$	$\alpha^{(qJ)}_{2n}$	$G_{33}(k,0)$ (ps)	$[D_T(k,0)]_{fJ}$ (Å^2/ps)
					(b)				
1	0.2877	25.1	9.20	25.8	45.9	1.282	−0.442	1.992	6.06
3	0.4983	15.4	9.08	14.0	48.9	1.366	−0.774	1.023	3.94
5	0.6432	38.6	3.92	21.0	52.5	0.580	−0.064	0.540	4.37
6	0.7046	33.1	4.46	18.4	51.6	0.599	−0.087	0.597	3.35
8	1.2865	64.0	4.51	18.5	55.3	0.247	−0.015	0.233	2.55
11	2.0744	33.8	1.38	15.2	45.4	0.418	0.072	0.0525	4.43
12	2.8766	24.6	6.45	17.1	46.0	0.618	0.038	0.0989	1.28

TABLE XI. Same as Table X (a) for model n [Eq. (5.13)].

No.	k (Å^{-1})	$[f_{Tq}^2]_{fn}$ (THz)^2	$\gamma_{1n}^{(q)}$ (THz)	$\gamma_{2n}^{(q)}$ (THz)	$\alpha_n^{(q)}$
1	0.2877	44.9	26.8	10.7	−0.46
3	0.4983	98.6	23.9	11.2	−0.67

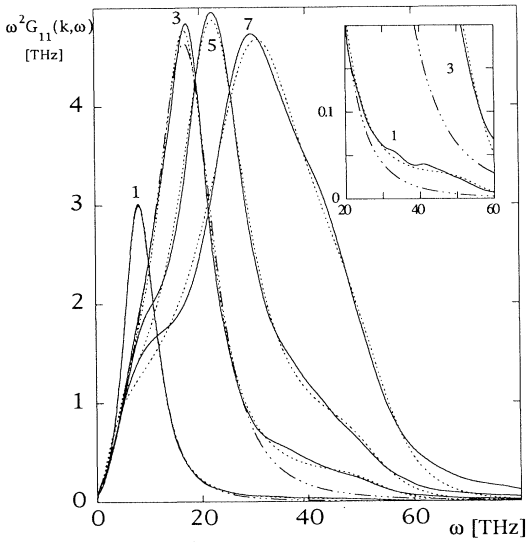

FIG. 11. Longitudinal current spectra computed directly (dotted curves) and from model J (solid curves) and model n (dot-dashed curves). The latter has been applied only to the two lowest k. The inset shows an enlarged view of the high-frequency region for the same two k ($T=245$ K).

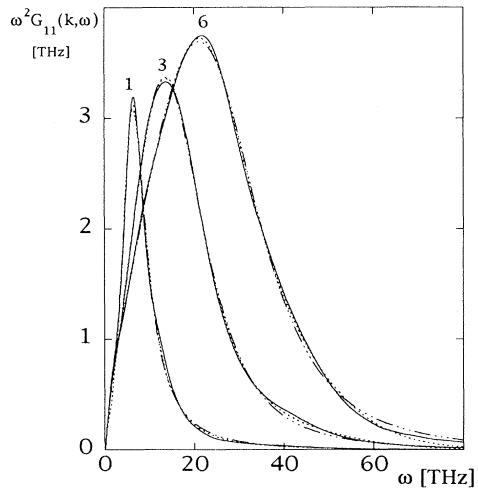

FIG. 12. Same as Fig. 11 at $T=298$ K.

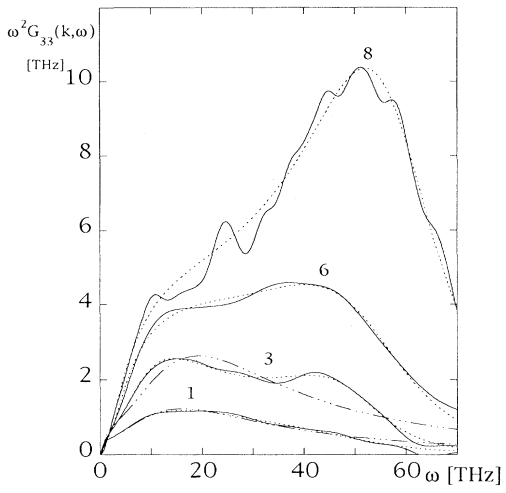

FIG. 13. Same as Fig. 12 for the spectrum of temperature-temperature ACF at 245 K.

$n_\sigma(k,t)$ and $n_q(k,t)$ from model J [$\alpha_{2n}^{(\sigma J)}(k)>0$ and $\alpha_{2n}^{(qJ)}(k)<0$] and from the results of model n [$\alpha_n^{(\sigma)}(k)>0$ and $\alpha_n^{(q)}(k)<0$].

From the data in the tables, it can also be seen that all parameters, except $f_{un}(k)^2$, $f_{u\sigma}(k)^2$, and $f_{Tq}(k)^2$, depend weakly on k^2. For example, $f_{un}(k)^2$ and $f_{u\sigma}(k)^2$ change by an order of magnitude in the k range spanned, as the theory predicts, while the other parameters change at most by $\sim 70-80\,\%$ in the same k range (Fig. 14). Hence it appears sensible to extrapolate these curves with a polynomial of the second degree in k^2, to estimate the behavior of $\omega^2 G_{11}(k,\omega)$ at low k values through Eqs. (5.6)–(5.8). The results of this fit also are shown in Fig. 14.

From the curve calculated at various k values, we obtain the frequency of the maximum $\omega_{\max}(k)$ and the width at half height of the acoustic mode peak $\delta\omega_{1/2}(k)$. The ratio $\omega_{\max}/k$ at 245 and 298 K is reported in Fig. 15(a) and $\delta\omega_{1/2}(k)/k^2$ at 245 K in Fig. 15(b).

It can be noted that the positive anomalous sound dispersion and the remarkable band narrowing begin between $k=0.01$ and 0.1 Å^{-1}. This is the same k range where $\gamma_{2n}^{(\sigma J)}(k)$, the decay rate of the long-time tail of $n_\sigma(k,t)$, becomes of the same order of magnitude as the frequency of the sound propagation peak. This holds true also for model n as the two models lead to very similar results in the $k,\omega\to 0$ limit.

By a polynomial extrapolation of the data reported in Table VIII, it is possible to predict the behavior of these functions at 298 K. The shape of the dispersion curve is slightly different from that at 245 K and shifted to larger k, a consequence of the shift to higher frequencies of the fitting parameters. At 298 K, $\omega_{\max}(k)$ and $\delta\omega_{1/2}(k)$ from the model can be compared to the neutron scattering results [3,4] [Figs. 16(a) and 16(b)]. The agreement is satisfactory, although the experimental $\omega_{\max}(k)$ is slightly underestimated, as already noted [10].

The computed sound velocities are 14±0.7 (run 1) and 15±0.7 (run 2) Å/ps at $T=245$ and 14.2±0.8 Å/ps and

298 K. As we do not calculate the isothermal compressibility χ_T, which determines $S(0)$, for simplicity the low-k behavior of $S(k)$ has been described with a polynomial fit on the data of run 2 ($f_{un}(k)^2=[k_BT/mS(k)]k^2=m_1k^2+m_2k^4$). This does not account for the rising of $S(k)$ in the low-k limit, observed experimentally in supercooled water, which leads to a lower sound speed at 245 K. This feature is much less apparent in our MD $S(k)$, as can be seen in the inset of Fig. 7.

Besides the almost quantitative agreement at room temperature, the qualitative trends at both temperatures can be explained by a simple extrapolation of the parameters that determine the k and ω dependence of the generalized viscosity.

Thus we can conclude that at the k values typical of neutron scattering and simulation, the sound velocity is 2–3 times larger and the bandwidth an order of magnitude smaller than those predicted by a simple extension of the hydrodynamic values. Besides the frequency dependence of $\tilde{n}(k,z)$, the physical quantity that plays the major role in determining the dispersion curve is the ratio [9,10]

$$\frac{[\omega_\infty(k)^2-\omega_0(k)^2]^{1/2}}{\omega_0(k)}\cong\frac{f_{u\sigma}(k)}{f_{un}(k)}\approx 3\ , \tag{6.1}$$

which is much higher than in most other liquids. $\omega_0(k)$ and $\omega_\infty(k)$ are the second moments of $G_{11}(k,t)$ and $G_{22}(k,t)$, respectively. The importance of the value of this ratio can easily be checked by repeating the calculation done to get the results of Figs. 15 and 16, with a smaller value of $f_{u\sigma}(k)$. Qualitatively, a dispersion curve of the same shape would be obtained at the larger k's, but the size of the dispersion would diminish and the bandwidth would increase linearly with the value of the ratio of Eq. (6.1).

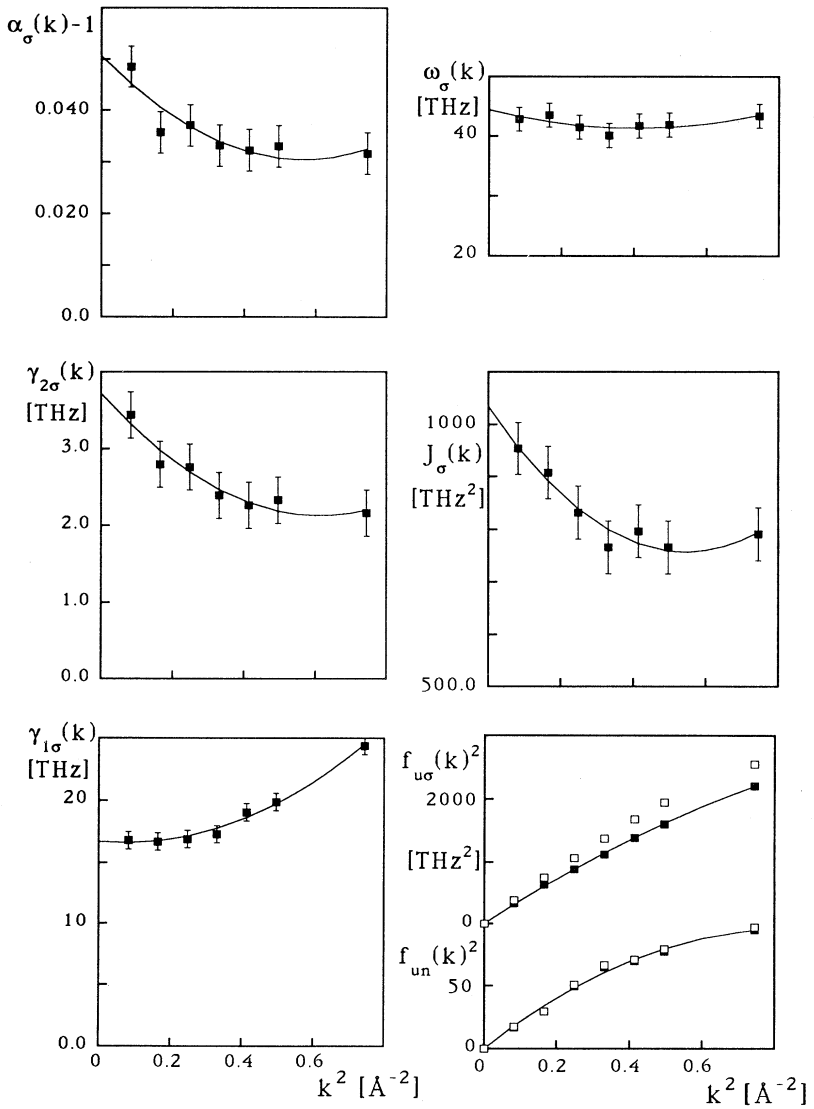

FIG. 14. k^2 dependence of the fitting parameters for model J applied to the density-density ACF at 245 K. The curve is a polynomial fit of the discrete values (solid squares). The error bar corresponds to the standard deviation. In the case of $f_{u\sigma}(k)^2$ and $f_{un}(k)^2$ (bottom right) the open squares are calculated values; see Table VI.

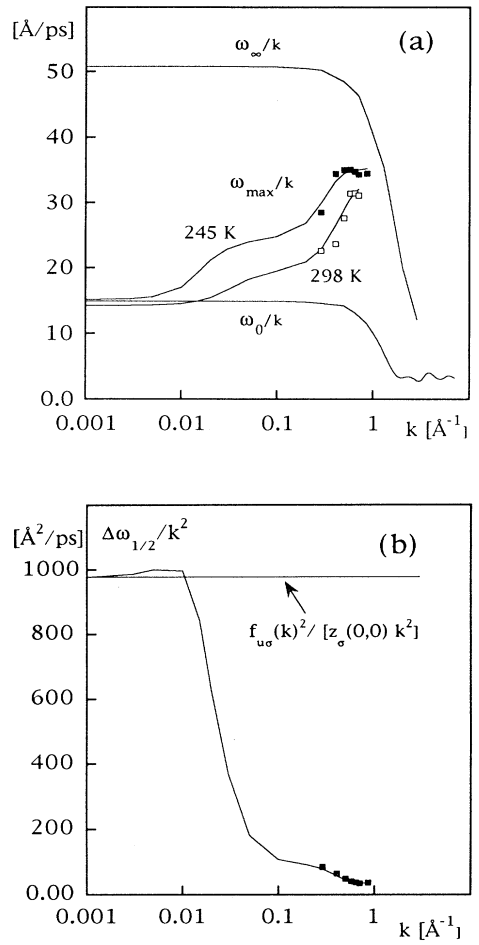

FIG. 15. (a) Dispersion curves for the acoustic mode, calculated from model J at 245 and 298 K. The solid and open squares are the MD values at the same two temperatures calculated from the Laplace transform of CF's of Figs. 1 and 2. The second moment of the longitudinal current ACF (ω_∞/k) and of the density-density ACF (ω_0/k) are also shown for $T=245$ K. (b) Width at half height calculated from model J at 245 K. The solid squares are MD values from CF's of Figs. 1 and 2 at 245 K. The horizontal line is the hydrodynamic limit ($T=245$ K).

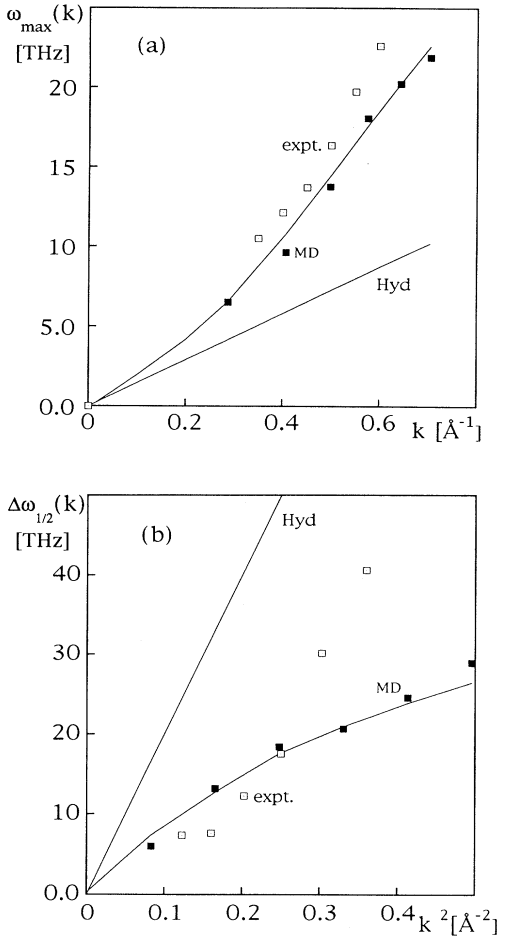

FIG. 16. (a) Comparison of experimental [3] (open squares) and MD results (solid squares) for the k dependence of the frequency of the maximum of the spectrum of the longitudinal current ACF. The curve shows the prediction from model J. The straight line is the hydrodynamic behavior ($T=298$ K). (b) Same as (a) for the width at half height.

VII. CALCULATION OF $n_\sigma(k,t)$, $n_q(k,t)$, $G_{44}(k,t)$, AND $G_{55}(k,t)$

With the knowledge of the generalized transport coefficients $z_\sigma(k,z)$ and $z_q(k,z)$ it is possible to calculate $n_\sigma(k,t)$ and $n_q(k,t)$ by means of Eqs. (5.1) and (5.2) at all k's. The results at $k=0.288$ Å^{-1} are compared in Figs. 17(a) and 17(b) with those obtained from model n with the parameters given in Table VII.

The main differences are visible at short time. The curve from model J has a vanishing derivative at $t=0$ and the oscillation due to the nearest-neighbor cage, features that are not included in model n. At longer times, on the other hand, there are only minor differences due to the different values of $[f_{un}(k)^2]_f$ and $[f_{u\sigma}(k)^2]_f$. Figure 17(a) and the inset also show $n_\sigma(k,t)$ computed directly from the simulation data through

$$\tilde{G}_{22}(k,z)\cong\frac{z}{z^2+f_{u\sigma}(k)^2\tilde{n}_\sigma(k,z)z+f_{un}(k)^2}\ . \tag{7.1}$$

The agreement between the function from model J and that obtained according to Eq. (7.1) is satisfactory, although some caution is necessary due to possible truncation effects on $\tilde{G}_{22}(k,z)$ from Eq. (7.1). As already noticed, $n_\sigma(k,t)$ has a positive long-time tail, while $n_q(k,t)$ a negative, faster, long-time tail.

$G_{44}(k,t)$ and $G_{55}(k,t)$, calculated by inversion of $\tilde{G}_{44}(k,z)$ and $\tilde{G}_{55}(k,z)$, as given by Eqs. (4.22) and (4.23), are shown in Figs. 18(a) and 18(b), where also $n_\sigma(k,t)$ and $n_q(k,t)$ are plotted. The latter are very similar to $G_{44}(k,t)$ and $G_{55}(k,t)$, respectively, as it should be expected, since these pairs of functions must be equal in the $k\to 0$ limit. In fact, $f_{un}(k)^2$ and $f_{u\sigma}(k)^2$ vanish as k^2, while $z_\sigma(k,z)$ and $z_q(k,z)$ go to a finite limit and depend weakly on k.

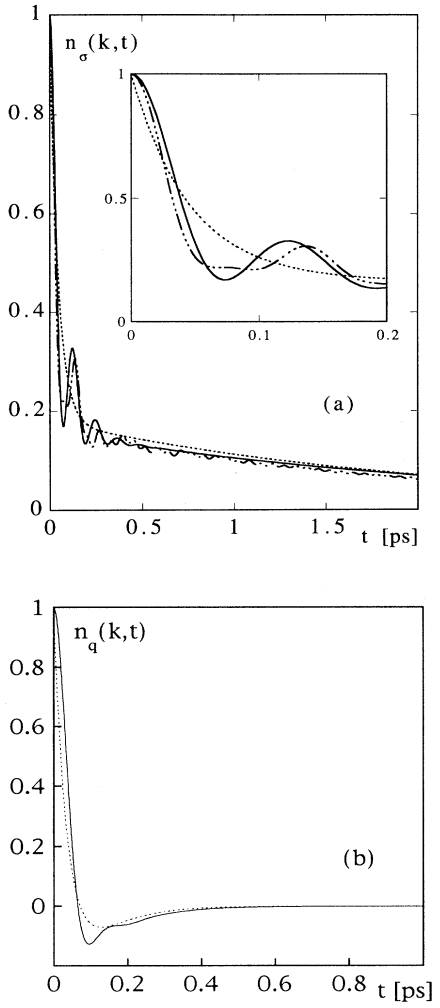

FIG. 17. (a) Longitudinal memory function $n_\sigma(k,t)$ from model J (solid line), model n (dotted line) and from an inversion of Eq. (7.1) (dash-dotted line). The inset shows an enlarged view of the short-time region ($T=245$ K, $k=k_{\min}$). (b) Temperature memory function $n_q(k,t)$ from model J (solid line) and (n) (dotted line) at 245 K and $k=k_{\min}$.

VIII. COLLECTIVE AND INDIVIDUAL DYNAMICS AND LONG-TIME TAILS

Recently [46], Kerr's theory [47] has been applied to calculate the time correlation functions of collective variables from the corresponding self-part. Other authors [48,49] have obtained, for the spectrum of the collective part, a relation with that of the self-function that is equivalent to Kerr's:

$$\tilde{G}_{11}(k,z)=\frac{[\tilde{G}_{11}(k,z)]^{\text{self}}}{1+\dfrac{S(k)-1}{S(k)}\{z[\tilde{G}_{11}(k,z)]^{\text{self}}-1\}} \quad (8.1)$$

It is clear that when $S(k)\equiv V_{11}(k)=1$ the collective function reduces to its self-part. From Fig. 19 it can be seen that this occurs in the case of water at $k=2$ Å^{-1}, i.e., when $S(k)\cong 1$. In this case, even the long-time decay rate $\lambda(k)$ of the self- and collective functions turns out quite similar.

From Fig. 20 one can also note that the acoustic mode band is hardly visible when $k>1$ Å^{-1}, as a consequence of its decreased amplitude and merging with the two bands corresponding to single-molecule modes. This is apparent from the figure, where the increase of amplitude of the O—O—O bending mode (8–10 THz), as a function of k, at the expense of the O—O stretching mode (40–50

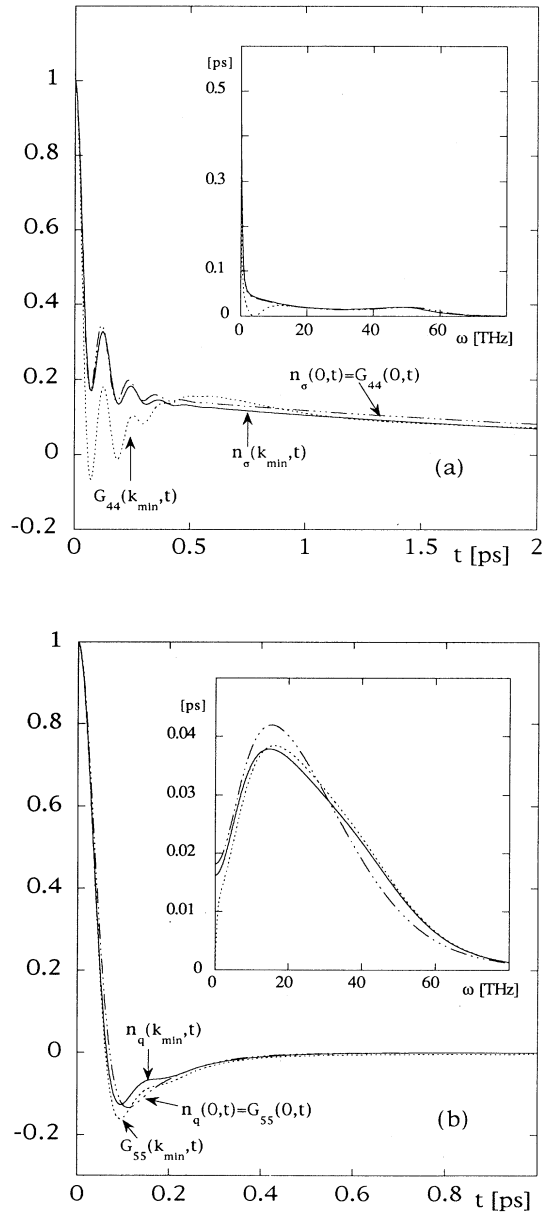

FIG. 18. (a) Comparison of the longitudinal memory function $n_\sigma(k,t)$ (solid line) with $G_{44}(k,t)$ (dotted line) at $k=k_{\min}$ and 0. In the latter case the two functions coincide (dot-dashed line) ($T=245$ K). The inset shows the corresponding spectra. (b) Same comparison for $n_q(k,t)$ and $G_{55}(k,t)$.

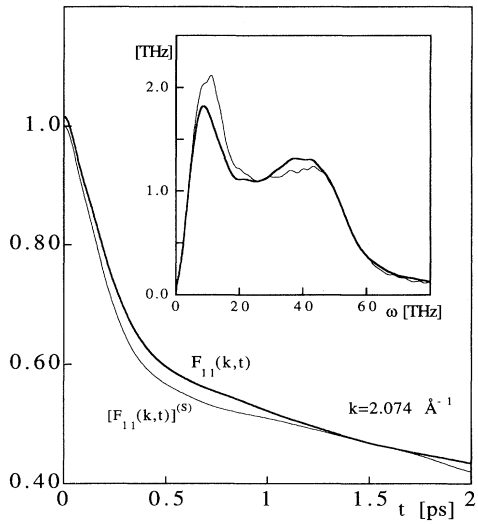

FIG. 19. Density-density ACF (bold line) and the corresponding self-part (thin line) at $k=2.074$ Å^{-1} at 245 K. The inset shows ω^2 times the corresponding spectra.

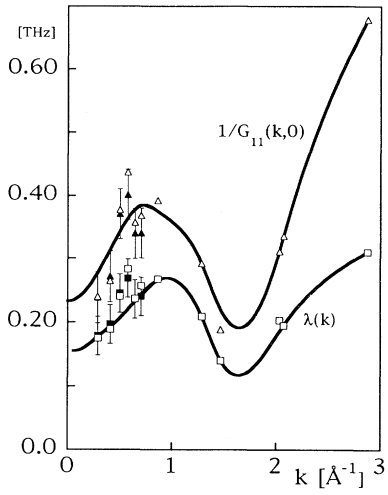

FIG. 21. Long-time decay rate $\lambda(k)$ and the inverse of the time integral of the density-density ACF at 245 K. Solid symbols relate to the average value of the two runs, while open symbols relate to the single runs; the curves are drawn as a guide.

THz) is clearly visible. The position of these two bands is not significantly dependent on k. This is why this low-frequency single-molecule mode does not affect much, at low k's, the collective density-density ACF, which can therefore be described satisfactorily by model J, although it does not take into account that mode. Including it in the model would require an additional combination of sine and cosine functions in Eq. (5.6), tuned on the frequency of the mode, 8–10 THz.

Another feature worth stressing is the lack of de Gennes narrowing [50] of the spectrum of $G_{11}(k,t)$ at $k\cong(2\pi/\sigma)\cong 2$ (σ is the length parameter in the LJ part of the TIP4P potential), where $S(k)$ has one of its maxima. Actually, $\lambda(k)$, the long-time decay rate of $G_{11}(k,t)$, reaches a minimum at a value of k that does not coincide with that of the maxima of $S(k)$ at room temperature [10].

$\lambda(k)$ is shown in Fig. 21 together with the inverse of the area under $G_{11}(k,t)$. There is an apparent correlation between the behavior of these two functions, which indicates that the long-time regime is also affected by the way $z_\sigma(k,0)$ depends on k

$$\frac{1}{\tilde{G}_{11}(k,\omega=0)}=\frac{f_{un}(k)^2}{f_{u\sigma}(k)^2}z_\sigma(k,\omega=0)\ . \tag{8.2}$$

When $k<1$ Å^{-1}, the ratio of the f's above is 0.09–0.08 at 245 K and does not vary much; see Table VI (the minimum is 0.03 at $k=2$ Å^{-1}). $z_\sigma(k,0)$, conversely, increases monotonically with k, from 2.35 THz at $k=k_{\min}$ to 12 THz at $k=10k_{\min}$. The combination of these two trends produces the results of Fig. 21 and shifts the minimum of $\lambda(k)$ from the k corresponding to the maximum of $S(k)$. As we shall see, this behavior is related to the fact that $\lambda(k)$ does not depend on thermal diffusivity.

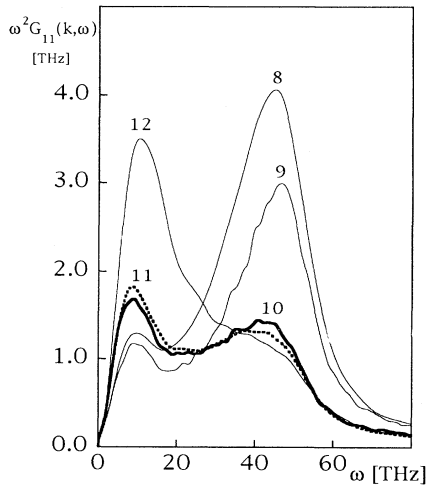

FIG. 20. Spectra of the longitudinal current ACF. The curves are labeled according to the value of k, reported in Table X (9 and 10 relate to $k=1.467$ and 2.034 Å^{-1}, respectively).

IX. TRANSVERSE CURRENTS

With the procedure outlined above it is possible to calculate the Laplace transform of the transverse current ACF $C_\perp(k,t)$, shown in Fig. 5. As discussed in [12], according to hydrodynamic theory this transform can be written as

$$\tilde{C}_\perp(k,z)=\frac{C_\perp(k,0)}{z+\omega_\perp(k)^2\tilde{n}_\perp(k,z)}\ , \tag{9.1}$$

where

$$\omega_\perp(k)^2=-\lim_{t\to 0}\frac{\partial^2[C_\perp(k,t)/C_\perp(k,0)]}{\partial t^2}\ . \tag{9.2}$$

The memory kernel used in [12] to fit the real part of this function is a combination of two exponentials

$$\tilde{n}_\perp(k,z)=\frac{1-\alpha_n^{(\perp)}(k)}{z+\gamma_{1n}^{(\perp)}(k)}+\frac{\alpha_n^{(\perp)}(k)}{z+\gamma_{2n}^{(\perp)}(k)} \ . \tag{9.3}$$

By analogy with $\tilde{G}_{33}(k,z)$ [see Eq. (4.21)], a memory kernel with the correct short-time behavior could be

$$\tilde{n}_\perp(k,z)\equiv\frac{1}{z+z_\perp(k,z)} \ , \tag{9.4}$$

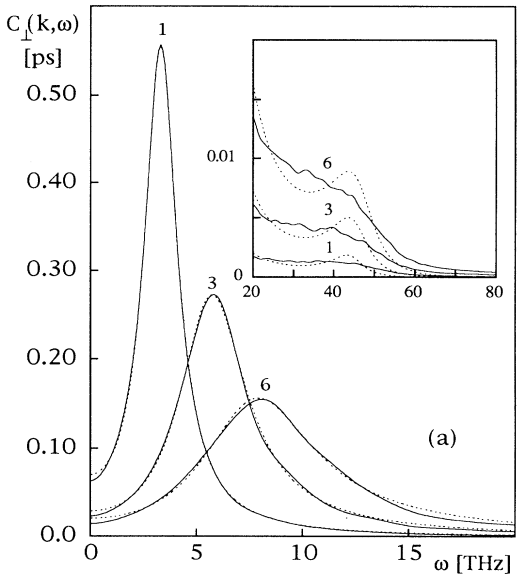

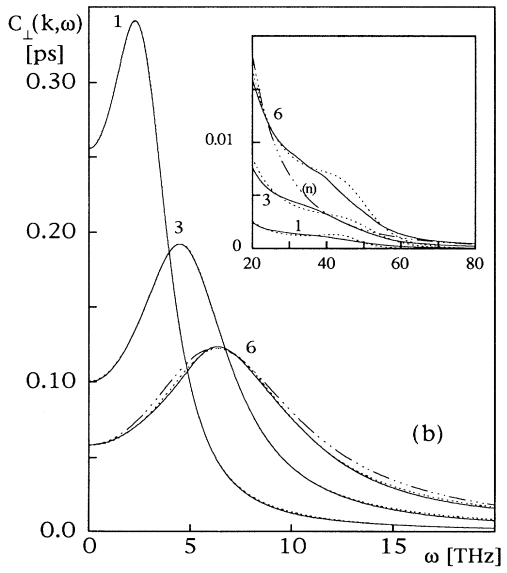

FIG. 22. (a) Spectra of the transverse current ACF at 245 K, computed directly (solid curve) and from model J (dotted curve). The inset details the high-frequency part. (b) Same as (a) at 298 K. The results from model n are shown for curve 6 ($k=0.705$ Å^{-1}).

where

$$\frac{z_\perp(k,z)}{J_\perp(k,0)}=\frac{z^2+a_{1J}^{(\perp)}(k)z+a_{0J}^{(\perp)}(k)}{z^3+a_{1J}^{(\perp)}(k)z^2+b_{1J}^{(\perp)}(k)z+b_{0J}^{(\perp)}(k)} \tag{9.5}$$

and $a_{1J}^{(\perp)}(k)$, $a_{0J}^{(\perp)}(k)$, $b_{1J}^{(\perp)}(k)$, and $b_{0J}^{(\perp)}(k)$ can be obtained from the coefficients $\gamma_{1J}^{(\perp)}(k)$, $\gamma_{2J}^{(\perp)}(k)$, $\omega_J^{(\perp)}(k)$, and $\alpha_J^{(\perp)}(k)$ by means of equations analogous to Eq. (5.9).

The results of the fit to $C_\perp(k,\omega)\equiv\mathrm{Re}\{\tilde{C}_\perp(k,z)/C_\perp(k,0)\}$ by equations of the form (5.17)–(5.19) are shown in Figs. 22(a) and 22(b) and the optimized parameters collected in Tables XII–XV.

As can be seen from the figure, $\omega_{\max}^{(\perp)}(k)$, the frequency of the maximum of $C_\perp(k,\omega)$, increases with k, while the height of the maximum decreases with k. Here too, the single-molecule band at 45 THz is more apparent when k increases.

It is worth stressing that a fit by model n with unconstrained parameters gives sensible results only at the first three values of k at $T=245$ K. It can be seen from Tables V–VII that $\omega_\perp(k)^2$, if unconstrained, would take much too high values after the first three k, to "compensate" for the band at 45 THz. Hence we chose to set it at the value obtained by Eq. (9.2). The optimized parameters for the fit with model J, on the other hand, behave regularly, although the unconstrained $\omega_\perp(k)^2$ is 30–40 % smaller than that given by Eq. (9.2).

X. VISCOSITY AND THERMAL CONDUCTIVITY

Total viscosity ($\frac{4}{3}\eta+\zeta$) and thermal diffusivity (D_T) can be obtained, extrapolating to $k=0$ the parameters reported in Tables VI, VIII, and X, by the following equations:

$$\tfrac{4}{3}\eta+\zeta=\lim_{k\to0}\frac{[f_{u\sigma}(k)^2]_f}{k^2z_\sigma(k,0)}=\lim_{k\to0}\frac{[f_{u\sigma}(k)^2]_f}{k^2}\tilde{n}_\sigma(k,0) \ , \tag{10.1}$$

$$D_T=\lim_{k\to0}\frac{[f_{Tq}(k)^2]_f}{k^2z_q(k,0)}=\lim_{k\to0}\frac{1}{k^2\tilde{G}_{33}(k,0)} \ . \tag{10.2}$$

From the first of Eqs. (4.7) thermal conductivity λ_T can be obtained. Moreover, from

$$\eta=\lim_{k\to0}\frac{[\omega_\perp(k)^2]_f}{k^2z_\perp(k,0)}=\lim_{k\to0}\frac{1}{k^2C_\perp(k,\omega=0)} \tag{10.3}$$

and

$$G_\infty=\lim_{k\to0}\frac{\rho\omega_\perp(k)^2}{k^2} \ , \tag{10.4}$$

the shear viscosity and the rigidity modulus can be calculated [12].

A polynomial extrapolation has been carried out on the data of Tables VI–XV for $k<1$ Å^{-1}. Theory allows us to set the zero-order term equal to zero when fitting $f_{u\sigma}(k)^2$, $f_{Tq}(k)^2$, and $\omega_\perp(k)^2$, while $z_\sigma(0,0)$, $z_q(0,0)$, and $z_\perp(0,0)$ do not vanish at $k=0$. The results obtained and the experimental data are collected in Table XVI at 245 and 298 K.

TABLE XII. (a) Computed (c) and optimized generalized frequencies and parameters used to fit $C_\perp(k,\omega)$ with model J [with a relation such as Eq. (5.17)]. (b) Coefficients required to compute $n_\perp(k,t)$. These values have been obtained from (a) as described in the Appendix ($T=245$ K). The last two columns are the frequency of the maximum and the time integral of the transverse current ACF.

No.	k (Å^{-1})	$[\omega_\perp^2]_{fJ}$ (THz)^2	$[\omega_\perp^2]_c$ (THz)^2	$J_\perp$ (THz)^2	$\gamma_{1J}^{(\perp)}$ (THz)	$\gamma_{2J}^{(\perp)}$ (THz)	$\omega_J^{(\perp)}$ (THz)	$\alpha_J^{(\perp)}$
				(a)				
1	0.2877	54.7	87	1049.3	10.4	7.5	29.3	1.1490
2	0.4067	110.5	174	1068.5	11.6	8.5	29.0	1.1915
3	0.4983	163.6	253	1073.2	13.3	9.3	28.8	1.2447
4	0.5754	214.4	335	1163.9	14.8	8.8	31.8	1.1998
5	0.6432	267.4	406	1079.8	16.0	11.4	28.0	1.3691
6	0.7046	314.8	472	1078.8	17.4	11.3	28.0	1.3867

No.	k (Å^{-1})	$\gamma_{1n}^{(\perp J)}$ (THz)	$\gamma_{2n}^{(\perp J)}$ (THz)	$\gamma_{3n}^{(\perp J)}$ (THz)	$\omega_n^{(\perp J)}$ (THz)	$\alpha_{2n}^{(\perp J)}$	$\alpha_{2n}^{(\perp J)}$	$\omega_{\max}^{(\perp)}$ (THz)	$[C_\perp(k,0)]_{fJ}$ (ps)
					(b)				
1	0.2877	17.81	0.7923	4.839	44.20	0.2608	0.1901	3.3	0.0704
2	0.4067	20.13	0.9451	5.537	44.39	0.2524	0.1903	4.7	0.0412
3	0.4983	22.69	0.9605	6.140	44.44	0.2511	0.1873	5.8	0.0288
4	0.5754	22.96	1.0887	7.119	47.29	0.2821	0.1855	6.9	0.0247
5	0.6432	27.38	1.3309	7.333	44.43	0.2355	0.1931	7.4	0.0232
6	0.7046	28.69	1.3557	7.973	44.43	0.2421	0.1869	8.4	0.0206

Thermal conductivity has been calculated only at 245 K, where the energy-energy and the density-energy correlation function have been computed. The value we obtain is in fairly good agreement with the experimental data. The latter has been extrapolated from data measured on the saturation curve between 543 and 273 K [51], as values measured in the supercooled region are not available.

The simulation result for thermal conductivity corresponds to a thermal diffusivity $D_T=7.8$ Å^2/ps. The comparison of this result with that of Fig. 21 shows that the long-time decay rate of $G_{11}(k,t)$ has no relation with the hydrodynamic prediction $[\lambda(k)=\omega_T(k)=D_T k^2]$. In this case, $\lambda(k)$ would vanish as k^2 and one should have $\lambda(k)=0.65$ THz at $k=k_{\min}=0.2877$ Å^{-1} and $\lambda(k)=7.8$ THz at $k=1$ Å^{-1}, much higher values than that of Fig. 21, but of the same order of magnitude as $1/\tilde{G}_{33}(k,0)$; see Table X.

At $\gamma=1$, the long-time decay rate of $G_{11}(k,t)$ is determined by generalized viscosity rather than thermal diffusivity. The latter is to be calculated from $G_{33}(k,t)$, i.e., extrapolating the data of Table X to $k=0$.

The dynamics underlying the viscosity with the TIP4P model turns out to be 30–40 % faster than in real water at room temperature and 2–3 times in the supercooled region, as also shown by self-diffusion and dielectric relaxation results [34,52]. All this is consistent with the observation that $D\eta/T \cong D\tau_D \cong$ const [53,54].

TABLE XIII. Same as Table XII for model n (see text).

No.	k (Å^{-1})	$[\omega_\perp^2]_{fn}$ (THz)^2	$\gamma_{1n}^{(\perp)}$ (THz)	$\gamma_{2n}^{(\perp)}$ (THz)	$\alpha_n^{(\perp)}$
1	0.2877	60.4	75.3	0.822	0.1223
2	0.4067	325	81.3	0.999	0.1234
3	0.4983	1083	82.0	1.012	0.1216
4	0.5754		79.7	1.185	0.1215
5	0.6432		83.2	1.314	0.1216
6	0.7046		79.5	1.306	0.1168

XI. SUMMARY AND CONCLUSIONS

In this paper, we have examined the density-density, energy-density, and energy-energy time correlation functions for the TIP4P model of water at 245 K. From the equal-time values of these functions, the generalized thermodynamic coefficients have been obtained. Moreover, fitting their Laplace transform by means of a model for the transport coefficients, important information around the propagation and dispersion of acoustic modes has been obtained. The main results we have obtained can be summarized as follows.

(i) $S(k)$ shows a neat peak at 2 Å^{-1}, which is a consequence of the increased, intermediate-range, tetrahedral ordering allowed by the lower temperature. At 298 K this peak is only a shoulder of the main peak at 3 Å^{-1}. The experimentally observed rise of the $S(k)$ curve when k goes to 0, related to correlated density fluctuations, is much less apparent in the MD results.

The specific heat capacity both at constant volume and pressure increases when k decreases in a way that makes their ratio very close to 1 when $k<1$ Å^{-1}. This is consistent with the very small value obtained for the thermal expansivity, which becomes negative for $k<0.45$ Å^{-1}, although the value extrapolated to $k=0$ is less negative than the experimental data [41]. This behavior and some other features such as the self-diffusion coefficient [24,29] and the dielectric relaxation times [29,34,52] indicate that the TIP4P model tends to underestimate the effect of a lower temperature on static and dynamic properties.

TABLE XIV. Same as Table XII at $T=298$ K.

No.	k (Å^{-1})	$[\omega_\perp^2]_{fJ}$ (THz)^2	$[\omega_\perp^2]_c$ (THz)^2	$J_\perp$ (THz)^2	$\gamma_{1J}^{(\perp)}$ (THz)	$\gamma_{2J}^{(\perp)}$ (THz)	$\omega_J^{(\perp)}$ (THz)	$\alpha_J^{(\perp)}$
1	0.2875	54.6	82	1172	18.0	9.4	29.1	1.224
2	0.4066	98.0	154	1066	15.8	7.3	29.1	1.137
3	0.4979	156.8	234	1200	25.5	10.4	27.7	1.338
4	0.5750	205.8	295	1206	25.5	10.6	26.0	1.393
5	0.6428	248.8	366	1131	23.4	12.9	25.1	1.517
6	0.7041	312.0	435	1293	32.0	11.4	26.0	1.414

No.	k (Å^{-1})	$\gamma_{1n}^{(\perp J)}$ (THz)	$\gamma_{2n}^{(\perp J)}$ (THz)	$\gamma_{3n}^{(\perp J)}$ (THz)	$\omega_n^{(\perp J)}$ (THz)	$\alpha_n^{(\perp J)}$	$\alpha_{2n}^{(\perp J)}$	$\omega_{\max}^{(\perp)}$ (THz)	$[C_\perp(k,0)]_{fJ}$ (ps)
1	0.2875	26.73	2.684	7.950	45.57	0.2744	0.1432	2.2	0.2560
2	0.4066	21.95	2.558	7.180	43.96	0.3108	0.1277	3.2	0.1421
3	0.4979	36.68	2.927	10.96	45.37	0.2552	0.1340	4.0	0.1006
4	0.5750	37.90	2.860	10.44	44.78	0.2337	0.1276	5.1	0.0791
5	0.6428	36.66	3.388	9.795	43.67	0.2195	0.1515	6.2	0.0657
6	0.7041	46.01	3.320	12.99	46.01	0.2213	0.1277	6.4	0.0579

Also the temperature dependence of the viscosities (Table XVI) confirms this limit of the TIP4P model.

(ii) The results in the hydrodynamic limit help to illustrate the ambiguous interpretation of the physical meaning of functions used to fit the density-density ACF. In particular, the effect of an increase of $\gamma(k)$ can be misunderstood as a frequency dependence of the generalized viscosity, unless the energy-density and the energy-energy time correlation function are also calculated. The behavior of the latter correlation functions has shown that, for water, it is the frequency dependence of the generalized viscosity that plays the major role to determine the observed anomalous sound dispersion, as $\gamma(k)\approx 1$. A further consequence of $\gamma(k)\approx 1$ is that, unlike in argon, $f_{uT}(k)$ behaves differently from the others, which increase linearly with k, at small k's.

(iii) The $\tilde{G}_{13}(k,z)$ has a small amplitude up to $k\approx 1$ Å^{-1} (see Fig. 10), which indicates that $\gamma(k)\approx 1$ and $|z_{q\sigma}(k,z)|$ is small [Eq. (3.24)]. Equations (3.23)–(3.27) in this case can be simplified and reduced to Eqs. (4.19)–(4.23), showing that density and temperature fluctuations are not coupled, the former being driven by the generalized viscosity term and the latter by the thermal diffusivity.

(iv) In view of the substantial dependence on frequency, in the case of water, of the generalized transport coefficients $z_\sigma(k,z)$ and $z_q(k,z)$, a simple viscoelastic model, with frequency-independent transport coefficients, turns out to be inadequate for this liquid.

(v) Model J for the generalized transport coefficients $z_\sigma(k,z)$, $z_q(k,z)$, and $z_\perp(k,z)$, introduced in this paper, allows us to accurately fit the spectra of the density-density, temperature-temperature, and longitudinal and transverse current ACF's also leading to a correct description of the short-time behavior, at least up to $k\cong 1$ Å^{-1}.

(vi) The optimized generalized frequencies of the fit agree satisfactorily with those obtained independently from the second moments or the initial values of the relevant ACF. The difference, which does not depend on k, is larger in the transverse functions and is due to the neglect of librational contributions [35].

(vii) The weak k^2 dependence of the fitting parameters allows a polynomial extrapolation to $k=0$ that gives both the large dispersion and the remarkable narrowing of the band of the acoustic mode, observed at the lowest k accessible to neutron diffraction and computer simulation.

As Fig. 15(a) shows, at 245 K there are two ranges of k where the speed of sound increases rapidly, separated by a plateau region. After this paper has been submitted, MD results by Sciortino and Sastry [55] on the TIP4P model at various temperatures have extended the analyses of sound dispersion down to $k=0.026$ Å^{-1}, i.e., at the edge of the plateau region of Fig. 15(a). There is a remarkable overall agreement between their MD data and the prediction of our model. The temperature effect also is that obtained with our model. It is particularly noticeable that at $k=0.026$ Å^{-1} (see Fig. 5 of [55]), the speed of sound ($\omega_{\max}/k$) is still twice as large as in the hydrodynamic limit (26 Å/ps vs 13 Å/ps), in the supercooled region. This supports the results of Fig. 15(a), i.e., that about 60–70 % of the dispersion occurs between 0.01 and 0.03 Å^{-1}.

From a physical point of view, these features are to be traced back to the large value of the second moment of the longitudinal current, which determines the overall size of the effect [see Eq. (6.1)], and to the slow decay

TABLE XV. Same as Table XIII at 298 K.

No.	k (Å^{-1})	$\gamma_{1n}^{(\perp)}$ (THz)	$\gamma_{2n}^{(\perp)}$ (THz)	$\alpha_n^{(\perp)}$
1	0.2875	73.3	2.66	0.0936
2	0.4066	69.0	2.61	0.0840
3	0.4979	71.6	2.73	0.0808
4	0.5750	71.0	2.61	0.0775
5	0.6428	72.0	3.04	0.0866
6	0.7041	66.9	2.86	0.0728

TABLE XVI. Comparison of calculated and experimental (in parentheses) thermal conductivity and viscosity and rigidity modulus.

T (K)	λ_T (W/mK)	$4\eta/3+\zeta$ (10^{-2} g/cm s)	η (10^{-2} g/cm s)	G_∞ (g/cm s^2)
245	0.35±0.07 (0.45)	10±2 (27)	2±0.3 (8)	(11.0±1.5) 10^{10}
298		2.0±0.5 (3)	0.5±0.15 (0.9)	(9.7±2) 10^{10}

$\gamma_{2n}^{(\sigma J)}(k)$ and amplitude $\alpha_{2n}^{(\sigma J)}(k)$ of the memory kernel $n_\sigma(k,t)$, that determine, respectively, the k range (0.01–0.03 Å^{-1} at 245 K and 0.02–0.06 Å^{-1} at 298 K) and the height of the first step of the dispersion curve.

(viii) In water, the negligible coupling between sound propagation and thermal fluctuations leads to a simplified picture of the liquid dynamics. It is possible, in particular, to shed light on the physical meaning of some fitting parameters. For example, the weak k dependence of J_σ, J_q, and $J_\perp$, as results from Tables VI–XV, and their similar values are evidence that the short-time behavior is dominated by collision phenomena, as shown at the end of Sec. V, and that τ_c depends weakly on k [56], at least in the low-k region. The collision time τ_c turns out to be 0.044 ps at 245 K and 0.037 ps at 298 K, in good agreement with simulation results (0.04 ps) for deuterated TIP4P water at 310 K [10].

As to the other parameters, $\gamma_{3n}^{(\sigma J)}(k)$ and $\omega_n^{(\sigma J)}(k)$ are related to the single-molecule mode determined by the oscillation of the tagged molecule in the nearest-neighbor cage, as is proved by the values of $\omega_n^{(\sigma J)}(k)$, always in the range 40–60 THz. It is also worth stressing that $\gamma_{3n}^{(\sigma J)}(k)$, the damping rate of this mode, roughly doubles at the higher temperature and this makes it more difficult to distinguish the single-molecule mode from the sound propagation mode.

The parameter $\gamma_{2n}^{(\sigma J)}(k)$, as already remarked in the previous sections, describes the long-time behavior of the memory functions and determines the shape of the dispersion curve, in the case of the density-density ACF. This parameter increase by a factor of 4 when temperature rises from 245 to 298 K (see Tables VI and VIII), a behavior opposite that of a typical structural time for this liquid. In Ref. [18] this long-time behavior is connected with mode-coupling effects, through the knowledge of structural properties.

As to the parameters used in the description of the spectra of the temperature-temperature ACF, $1/\gamma_{2n}^{(qJ)}(k)$ is much shorter than that relevant to the density-density and transverse current ACF, while the negative amplitude and long-time tail are fairly close to the corresponding values for the single-molecule velocity ACF. The other parameters $\gamma_{1n}^{(\sigma J)}(k)$, $\gamma_{1n}^{(qJ)}(k)$, and $\gamma_{1n}^{(\perp J)}(k)$ are of order $1/\tau_c(k)$ and are probably an extension to relatively intermediate times of binary collision effects.

(ix) $G_{44}(k,t)$ and $G_{55}(k,t)$ in the low-k region are very similar to the memory functions $n_\sigma(k,t)$ and $n_q(k,t)$ and should became equal in the limit $k=0$; see Fig. 18. It is also apparent that the single-molecule mode related to the oscillation in the nearest-neighbor cage remains more clearly visible in $G_{44}(k,t)$ than in $G_{55}(k,t)$. Work is in progress to identify the contribution to the longitudinal momentum and energy flux, which is responsible for this different behavior.

APPENDIX: CALCULATION OF $n_{\sigma,q,\perp}(k,t)$ FROM $J_{\sigma,q,\perp}(k,t)$

By Laplace transform of Eq. (5.20) we obtain

$$n_\sigma^{(J)}(k,z)=\frac{z^3+a_{2n}^{(\sigma J)}(k)z^2+a_{1n}^{(\sigma J)}(k)z+a_{0n}^{(\sigma J)}(k)}{z^4+a_{2n}^{(\sigma J)}(k)z^3+b_{2n}^{(\sigma J)}(k)z^2+b_{1n}^{(\sigma J)}(k)z+b_{0n}^{(\sigma J)}(k)}\ , \tag{A1}$$

where

$$\begin{aligned}
a_{2n}^{(\sigma J)}&=\gamma_{1n}^{(\sigma J)}+\gamma_{2n}^{(\sigma J)}+2\gamma_{3n}^{(\sigma J)}\ ,\\
a_{1n}^{(\sigma J)}&=\alpha_{1n}^{(\sigma J)}[\omega_n^{(\sigma J)^2}+(\gamma_{3n}^{(\sigma J)}-\gamma_{1n}^{(\sigma J)})^2]+\alpha_{2n}^{(\sigma J)}[\omega_n^{(\sigma J)^2}+(\gamma_{3n}^{(\sigma J)}-\gamma_{2n}^{(\sigma J)})^2]+2\gamma_{3n}^{(\sigma J)}(\gamma_{1n}^{(\sigma J)}+\gamma_{2n}^{(\sigma J)})+\gamma_{1n}^{(\sigma J)}\gamma_{2n}^{(\sigma J)}\ ,\\
a_{0n}^{(\sigma J)}&=\alpha_{1n}^{(\sigma J)}\gamma_{2n}^{(\sigma J)}[\omega_n^{(\sigma J)^2}+(\gamma_{3n}^{(\sigma J)}-\gamma_{1n}^{(\sigma J)})^2]+\alpha_{2n}^{(\sigma J)}\gamma_{1n}^{(\sigma J)}[\omega_n^{(\sigma J)^2}+(\gamma_{3n}^{(\sigma J)}-\gamma_{2n}^{(\sigma J)})^2]+2\gamma_{1n}^{(\sigma J)}\gamma_{2n}^{(\sigma J)}\gamma_{3n}^{(\sigma J)}\ ,\\
b_{2n}^{(\sigma J)}&=\gamma_{1n}^{(\sigma J)}(\gamma_{2n}^{(\sigma J)}+2\gamma_{3n}^{(\sigma J)})+\gamma_{3n}^{(\sigma J)^2}+\omega_n^{(\sigma J)^2}+2\gamma_{2n}^{(\sigma J)}\gamma_{3n}^{(\sigma J)}\ ,\\
b_{1n}^{(\sigma J)}&=(\gamma_{1n}^{(\sigma J)}+\gamma_{2n}^{(\sigma J)})(\omega_n^{(\sigma J)^2}+\gamma_{3n}^{(\sigma J)^2})+2\gamma_{1n}^{(\sigma J)}\gamma_{2n}^{(\sigma J)}\gamma_{3n}^{(\sigma J)}\ ,\\
b_{0n}^{(\sigma J)}&=\gamma_{1n}^{(\sigma J)}\gamma_{2n}^{(\sigma J)}(\omega_n^{(\sigma J)^2}+\gamma_{3n}^{(\sigma J)^2})\ .
\end{aligned} \tag{A2}$$

In Eqs. (A2) all parameters depend on k, though not explicitly indicated, to simplify notation.

From Eqs. (5.8), (5.1), and (5.9) we get an equation equal to Eq. (A1) with

$$\begin{aligned}
&a_{2n}^{(J)}(k)=a_{1J}^{(\sigma)}(k),\quad a_{1n}^{(J)}(k)=b_{1J}^{(\sigma)}(k),\quad a_{0n}^{(J)}(k)=b_{0J}^{(\sigma)}(k)\ ,\\
&b_{2n}^{(\sigma J)}(k)=b_{1J}^{(\sigma)}(k)+J_\sigma(k,0),\quad b_{1n}^{(\sigma J)}(k)=b_{0J}^{(\sigma)}(k)+a_{1J}^{(\sigma)}(k)J_\sigma(k,0),\quad b_{0n}^{(\sigma J)}(k)=a_{0J}^{(\sigma)}(k)J_\sigma(k,0)\ .
\end{aligned} \tag{A3}$$

By simple algebra, the following relations can be derived from Eq. (A2):

$$
\begin{aligned}
&\gamma_{1n}^{(\sigma J)^4}-a_{1J}^{(\sigma)}\gamma_{1n}^{(\sigma J)^3}+(b_{1J}^{(\sigma)}+J_\sigma)\gamma_{1n}^{(\sigma J)^2}-(b_{0J}^{(\sigma)}+J_\sigma a_{1J}^{(\sigma)})\gamma_{1n}^{(\sigma J)}+a_{0J}^{(\sigma)}J_\sigma=0\ ,\\
&\gamma_{2n}^{(\sigma J)^3}-(a_{1J}^{(\sigma)}-\gamma_{1n}^{(\sigma J)})\gamma_{2n}^{(\sigma J)^2}+[b_{1J}^{(\sigma)}+J_\sigma-\gamma_{1n}^{(\sigma J)}(a_{1J}^{(\sigma)}-\gamma_{1n}^{(\sigma J)})]\gamma_{2n}^{(\sigma J)}-\frac{a_{0J}^{(\sigma)}J_\sigma}{\gamma_{1n}^{(\sigma J)}}=0\ ,\\
&\gamma_{3n}^{(\sigma J)}=\frac{a_{1J}^{(\sigma)}-\gamma_{1n}^{(\sigma J)}-\gamma_{2n}^{(\sigma J)}}{2}\ ,\\
&\omega_n^{(\sigma J)}=\left[\frac{a_{0J}^{(\sigma)}J_\sigma}{\gamma_{1n}^{(\sigma J)}\gamma_{2n}^{(\sigma J)}}-\gamma_{3n}^{(\sigma J)^2}\right]^{1/2}\ ,\\
&\alpha_{1n}^{(\sigma J)}=\frac{\gamma_{1n}^{(\sigma J)}(\omega_n^{(\sigma J)^2}+\gamma_{3n}^{(\sigma J)^2}-J_\sigma)-b_{0J}^{(\sigma)}+2\gamma_{1n}^{(\sigma J)}\gamma_{2n}^{(\sigma J)}\gamma_{3n}^{(\sigma J)}}{(\gamma_{1n}^{(\sigma J)}-\gamma_{2n}^{(\sigma J)})[\omega_n^{(\sigma J)^2}+(\gamma_{3n}^{(\sigma J)}-\gamma_{1n}^{(\sigma J)})^2]}\ ,\\
&\alpha_{2n}^{(\sigma J)}=\frac{\gamma_{2n}^{(\sigma J)}(\omega_n^{(\sigma J)^2}+\gamma_{3n}^{(\sigma J)^2}-J_\sigma)-b_{0J}^{(\sigma)}+2\gamma_{1n}^{(\sigma J)}\gamma_{2n}^{(\sigma J)}\gamma_{3n}^{(\sigma J)}}{(\gamma_{2n}^{(\sigma J)}-\gamma_{1n}^{(\sigma J)})[\omega_n^{(\sigma J)^2}+(\gamma_{3n}^{(\sigma J)}-\gamma_{2n}^{(\sigma J)})^2]}\ ,
\end{aligned}
\tag{A4}
$$

where $J_\sigma \equiv J_\sigma(k,0)$.

Solving the first two equations of (A4), all six coefficients can be obtained. They must be real and $\gamma_{1n}^{(\sigma J)}(k)$, $\gamma_{2n}^{(\sigma J)}(k)$, $\gamma_{3n}^{(\sigma J)}(k)$, $\omega_n^{(\sigma J)}$ must be positive.

From Eq. (5.8), the following relations can easily be derived:

$$
\begin{aligned}
&\gamma_{2J}^{(\sigma)^3}-a_{1J}^{(\sigma)}\gamma_{2J}^{(\sigma)^2}+b_{1J}^{(\sigma)}\gamma_{2J}^{(\sigma)}-b_{0J}^{(\sigma)}=0\ ,\\
&\gamma_{1J}^{(\sigma)}=\frac{a_{1J}^{(\sigma)}-\gamma_{2J}^{(\sigma)}}{2}\ ,\\
&\omega_J^{(\sigma)}=\left[\frac{b_{0J}^{(\sigma)}-\gamma_{2J}^{(\sigma)}\gamma_{1J}^{(\sigma)^2}}{\gamma_{2J}^{(\sigma)}}\right]^{1/2}\ ,\\
&\alpha_J^{(\sigma)}=1+\frac{2\gamma_{1J}^{(\sigma)}\gamma_{2J}^{(\sigma)}-a_{0J}^{(\sigma)}}{\omega_J^{(\sigma)^2}+(\gamma_{1J}^{(\sigma)}-\gamma_{2J}^{(\sigma)})^2}\ .
\end{aligned}
\tag{A5}
$$

The coefficients can now be obtained by solving the first equation of (A5).

Hence, from the five parameters $a_{1J}^{(\sigma)}(k)$, $a_{0J}^{(\sigma)}(k)$, $b_{1J}^{(\sigma)}(k)$, $b_{0J}^{(\sigma)}(k)$, and $J_\sigma(k,0)$ the parameters relevant to model J can be calculated through Eqs. (A4) and (A5). Model n approximates Eq. (5.20) with a combination of two exponentials, so only the amplitude and the decay rate of the slower exponential, $\alpha_{2n}^{(\sigma J)}(k), \gamma_{2n}^{(\sigma J)}(k)$ and $\alpha_{2n}^{(\sigma)}(k), \gamma_{2n}^{(\sigma)}(k)$ can be directly compared; see Tables VI–XV.

[1] A. Rahman and F. H. Stillinger, Phys. Rev. A **10**, 368 (1974).

[2] R. W. Impey, P. A. Madden, and I. R. McDonald, Mol. Phys. **46**, 513 (1982).

[3] J. Teixeira, M. C. Bellisent-Funel, S. H. Chen, and B. Dorner, Phys. Rev. Lett. **54**, 2681 (1985).

[4] S. H. Chen and J. Teixeira, Adv. Chem. Phys. **64**, 1 (1985).

[5] Th. Kowall, P. Mausbach, and A. Geiger, Ber. Bunsenges. Phys. Chem. **94**, 279 (1990).

[6] M. Wojcik and E. Clementi, J. Chem. Phys. **85**, 6085 (1986).

[7] M. A. Ricci, D. Rocca, G. Ruocco, and R. Vallauri, Phys. Rev. A **40**, 7226 (1989).

[8] S. Sastry, F. Sciortino, and H. E. Stanley, J. Chem. Phys. **95**, 7775 (1991).

[9] U. Balucani, G. Ruocco, A. Torcini, and R. Vallauri, Phys. Rev. E **47**, 1677 (1993).

[10] U. Balucani, G. Ruocco, M. Sampoli, A. Torcini, and R. Vallauri, Chem. Phys. Lett. **209**, 408 (1993).

[11] D. Levesque, L. Verlet, and J. Kurkuijarvi, Phys. Rev. A **7**, 1690 (1973).

[12] D. Levesque and L. Verlet, Mol. Phys. **61**, 143 (1987).

[13] J. P. Hansen and I. R. McDonald, *Theory of Simple Liquids* (Academic, London, 1986).

[14] R. D. Mountain, Adv. Mol. Relaxation Processes **9**, 225 (1977).

[15] J. P. Boon and S. Yip, *Molecular Hydrodynamics* (McGraw-Hill, New York, 1980).

[16] W. E. Alley and B. Alder, Phys. Rev. A **27**, 3158 (1983).

[17] I. M. de Schepper, E. G. D. Cohen, C. Bruin, J. C. van Rijis, w. Montfrooij, and L. A. de Graaf, Phys. Rev. A **38**, 271 (1988).

[18] U. Balucani, Mol. Phys. **71**, 123 (1990).

[19] N. K. Ailawadi, A. Rahman, and R. Zwanzig, Phys. Rev. A **4**, 1616 (1971).

[20] J. R. D. Copley and S. W. Lovesey, Rep. Prog. Phys. **38**,

461 (1975).
[21] P. K. Kahol, R. Bansal, and K. N. Pathak, Phys. Rev. A **14**, 408 (1976).
[22] S. W. Lovesey, Phys. Rev. Lett. **53**, 401 (1984); Z. Phys. B **58**, 79 (1985).
[23] R. Zwanzig and M. Bixon, Phys. Rev. A **2**, 2005 (1970).
[24] D. Bertolini, M. Cassettari, M. Ferrario, P. Grigolini, G. Salvetti, and A. Tani, J. Chem. Phys. **91**, 1179 (1989); D. Bertolini, P. Grigolini, and A. Tani, *ibid.* **91**, 1191 (1989).
[25] W. L. Jorgensen, J. Chandrasekhar, J. D. Madura, R. W. Impey, and M. L. Klein, J. Chem. Phys. **79**, 926 (1983).
[26] G. Ciccotti, J. P. Ryckaert, and M. Ferrario, Mol. Phys. **47**, 1253 (1982).
[27] M. Ferrario and A. Tani, Chem. Phys. Lett. **121**, 182 (1985).
[28] W. L. Jorgensen and J. D. Madura, Mol. Phys. **56**, 1381 (1985).
[29] K. Watanabe and M. L. Klein, Chem. Phys. **131**, 157 (1989).
[30] R. C. Desai and R. Kapral, Phys. Rev. A **6**, 2377 (1972).
[31] M. Weinberg, R. Kapral, and R. C. Desai, Phys. Rev. A **7**, 1413 (1973).
[32] D. J. Evans, Mol. Phys. **32**, 1171 (1976); **42**, 1355 (1981); D. J. Evans and S. Murad, *ibid.* **68**, 1219 (1989).
[33] D. Bertolini, A. Tani, and R. Vallauri, Mol. Phys. **73**, 69 (1991); D. Bertolini and A. Tani, *ibid.* **75**, 1047 (1992); D. Bertolini, A. Tani, and D. Vitali, in *Proton Transfer in Hydrogen-Bonded Systems,* edited by T. Bountis (Plenum, New York, 1992).
[34] D. Bertolini and A. Tani, Mol. Phys. **75**, 1065 (1992).
[35] D. Bertolini and A. Tani (unpublished).
[36] L. P. Kadanoff and J. Swift, Phys. Rev. **166**, 89 (1968).
[37] M. H. Ernst and J. R. Dorfman, J. Stat. Phys. **12**, 311 (1975).
[38] M. H. Ernst, E. H. Hauge, and J. M. van Leeuwen, J. Stat. Phys. **15**, 7 (1976).
[39] J. Bosio, J. Teixeira, and H. E. Stanley, Phys. Rev. Lett. **46**, 597 (1981).
[40] Y. Xie, K. F. Ludvig, Jr., G. Morales, D. E. Hare, and C. M. Sorensen, Phys. Rev. Lett. **71**, 2050 (1993).
[41] D. E. Hare and C. M. Sorensen, J. Chem. Phys. **87**, 4840 (1987).
[42] M. Schoen, R. Vogelsang, and C. Hoheisel, Mol. Phys. **57**, 445 (1986).
[43] R. D. Mountain, Rev. Mod. Phys. **38**, 205 (1966).
[44] P. Schofield, in *Physics of Simple Liquids,* edited by H. N. V. Temperley, J. S. Rowlinson, and G. S. Rushbrooke (North-Holland, Amsterdam, 1968).
[45] U. Balucani, R. Vallauri, T. Gaskell, and S. F. Duffy, J. Phys. Condens. Matter **2**, 5015 (1990).
[46] D. Wei and G. N. Patey, J. Chem. Phys. **91**, 7113 (1989); **93**, 1399 (1990); **94**, 6785 (1991); **94**, 6795 (1991).
[47] W. C. Kerr, Phys. Rev. **174**, 316 (1968).
[48] K. S. Singwi, K. Skold, and M. P. Tosi, Phys. Rev. Lett. **21**, 881 (1968).
[49] K. Kim and M. Nelkin, Phys. Rev. A **4**, 2065 (1971).
[50] P. G. de Gennes, Physica **25**, 825 (1959).
[51] V. P. Isachenko, V. A. Osipova, and A. S. Sukomel, *Heat Transfer* (Mir, Moscow, 1977), p. 481.
[52] M. Neumann, J. Chem. Phys. **85**, 1567 (1986).
[53] H. R. Pruppacher, J. Chem. Phys. **56**, 101 (1972).
[54] D. Bertolini, M. Cassettari, and G. Salvetti, J. Chem. Phys. **76**, 3285 (1982).
[55] F. Sciortino and S. Sastry, J. Chem. Phys. **100**, 3881 (1994).
[56] L. Sjogren, J. Phys. C **13**, 705 (1980).